Gas Sensors Based on Atomically-Thin Field-Effect Transistors

モハメド, アミール, ビン, ズルケフリ

Gas Sensors Based on Atomically-Thin Field-Effect Transistors

Mohd Amir bin Zulkefli

Department of Chemistry and Biochemistry

Graduate School of Engineering

Kyushu University

2021

Table of Contents

Chapter 1
Introduction

1.1. Background

Nowadays, the industrial field and urban life are globalizing and growing rapidly. These trends cause severe air pollution due to the contamination of volatile organic compound (VOC) and toxic gases into the environment.[1,2] These gas molecules are toxic to human beings, animal, and the environment, even at low concentration exposure.[3,4] Additionally, this polluted air can cause serious health problems such as nerve damage and kidney failure after prolonged exposure and inhalation into the human body.[5] For this reason, the detection and monitoring of the air pollution are crucial for sustaining the environment and protecting the human life.

The conventional method and equipment for the detection and identification of gases are based on gas chromatography (GC) as well as electronic nose. These approaches and devices are relatively accurate and sensitive for molecule detection. Nevertheless, some issues and challenges need to be addressed such as expensive and sophisticated instrument with complex sample preparations, large equipment size, needs for expert manpower to operate GC, and selectivity issues in a gas mixture. To add, these methods are time-consuming and difficult to achieve in real-time applications especially for high-frequency air pollutants monitoring in a large area. Therefore, sensitive, selective, high-throughput gas detection with a simple device structure and real-time monitoring capabilities are highly essential to develop. In **Section 1.1.1**, an overview of the gas sensor technology is provided.

For these reasons, developments in alternative gas sensor technology are essential in terms of low-cost, small size, easy handling and operation as well as user-friendly sensing measurement. Alternative gas sensors are typically categorized into electrochemical-based, optical-based, pyroelectric-based, piezoelectric-based, and electrical-based sensor devices. Electrical-based sensors, for instance field-effect transistor (FET) structure, attracted much research attention. This is due to their intrinsic advantages such as well-developed fabrication process with low cost fabrication technique on a large area substrate, as well as favorably integrated into an electronic circuit. Moreover, current modulation by gate bias and room temperature operation provide the advantages of a long device lifetime and low power consumption.[6,7] A brief description of the FET structure, operation, and FET-based gas sensor devices are given in **Section 1.1.2**.

In addition, the FET structure with two-dimensional (2D) transition metal dichalcogenide (TMDC) has been developed for gas sensors because the TMDC films such as molybdenum disulfide (MoS_2) and tungsten disulfide (WS_2) have intrinsic advantage, i.e., high surface-area-to-volume ratio. However, the selective detection of gases remains challenging, especially for sensors using a 2D material-based single device. Therefore, exploring appropriate sensing materials and novel sensing concept to address the above-mentioned challenges are critical. The basic properties of 2D materials are introduced in **Section 1.1.3**.

Two possible techniques to address above issues are light illumination and gate biasing to 2D-TMDC FETs, through which the gas sensing properties could be significantly improved through photo-induced and capacitive-induced carriers for interaction with gas molecules.[3,8–10] However, owing to the limited material selection to

find balance and overcome the trade-off relationship between charge carrier density, light absorption (thick layer and direct bandgap material required) and high surface-area-to-volume ratio (thin layer required), insufficient research has been conducted on light-assisted and gate-bias tunability based on TMDC-FET structures for achieving gas-sensing efficiency and selectivity. Rhenium disulfide (ReS_2) has attracted attention in this regard because it exhibits a direct bandgap property regardless of thickness. Meanwhile, the thickness must be monolayer for the conventional TMDCs to get direct bandgaps[11–17]. Then, the light absorption become less effective. Therefore, ReS_2 is a promising material for overcoming the trade-off relation between the charge carrier density with the optical absorption (thick layer and direct bandgap material better) and high surface-area-to-volume ratio (thin layer better) for realizing a single-device operation of selective and sensitive gas sensors based on the effective response of ReS_2 to light illumination.[18,19] The advantages of 2D TMDC-FETs based gas sensor devices are discussed in **Section 1.1.4**.

1.1.1. Gas sensor technology

The atmospheric air contains numerous gases molecules. Some of them are vital in human life while many others are hazardous. Crucial gases like oxygen and humidity should be maintained at adequate level. Meanwhile, emission of hazardous gases should be controlled at safety level. Such monitoring, controlling and handling of these gases are doable only when the concentration of each gas can be detected in a real-time condition. In this manner, gas sensors are essential components of sensing systems due to their broad range of applications in medical field, environmental monitoring, and industrial field.[20]

For these purpose, it is vital to detect numerous kinds of gas molecules for field applications.

The conventional GC, in combination with a numerous of detectors such as flame ionization (FID), mass spectroscopy (MS), photo-ionization detectors (PID), thermal conductivity detectors (TCD) as shown in **Figure 1-1** is the widely applied approach for monitoring the complex gaseous mixtures.[21] These methods have several advantages such as high sensitivity and accuracy. However, real-time field monitoring using a conventional GC encounter a lot of fundamental challenges due to its heavy equipment weight, complex operation procedure, large size, requirement for specific carrier gases, etc. Besides, huge carrier gas tanks are needed to be attached to the instrument, which limit the device portability. Besides, the device also faces challenge in selectivity in a wide variety of gases mixtures.

Figure 1-1. gas chromatography-mass spectrometer.

(Reproduced from The Summons Lab., https://summons.mit.edu)

For that reason, there is an ongoing process of developing alternative gas sensing methods such as electrochemical-based, optical-based, pyroelectric-based, piezoelectric-based, and electrical-based sensor devices, whereby the sensing materials can change their electronic, electrical, and optical properties upon gas exposure, which represent the

sensing signal. For instance, when the *n*-type semiconductor sensing layer is exposed to reducing gases like ethanol, etc., the conductivity of the device increases. These changes on the conductivity of the sensing materials are due to the two possible mechanisms. Firstly, in the case of conventional metal-oxide-based sensors, when the sensing operation is at temperature higher than 100°C, oxygen ions adsorb on the sensing layer surface which later on interact with the target gas molecule. For example, in the CO gas sensor, a CO molecule interacts with an oxygen ion on the surface of the sensing layer, resulting in its oxidation, forming CO_2 and releasing one electron on the sensing layer surface. Thus, the conductivity of sensor device (*n*-type material) is increased. Contrary, when gas molecules (acceptor gas) accept electrons, decreasing in the *n*-type material conductivity is induced.[20,22] Another mechanism is the charge transfer, which does not involve the adsorption of the oxygen ions, whereby the gas molecules adsorbed on the sensing layer surface, and a charge carrier transfer occur between gas molecule and sensing layer, which depend on the type of sensing material and gas molecule.

There are several parameters used for evaluating the sensor performances such as sensor response, operating temperature, selectivity to a certain gas, and long-term stability and reliability. The sensor response is defined as the relative changes of the sensing signal when the gas molecule is introduced into the test chamber. Another vital parameter is the operating temperature for the sensor commercialization purpose. The conventional metal-oxide-based sensor works at high temperature (>100°C). At these conditions, the oxygen molecules are adsorbed on the surface, thus interact with gas molecules, stimulating the change of electrical parameter of the sensor device. Nevertheless, high sensing temperature operation increases the power consumption of the sensor devices. Therefore, in the past few years, the gas sensing development is focused on the room temperature

sensing operation. Selectivity to a certain gas in a mixture of other gases is another important parameter of gas sensor performance. In normal conditions, the sensors are exposed to mixture of different gases. In this regard, the selectivity of a sensor can be estimated under the condition of numerous gas exposure and by measuring the responses of each gas. Then, the reliability and stability are another key factor of the gas sensor in which the response of the sensor device should not change over time. All of these parameters should be considered for developing high performance gas sensor.

1.1.2. FET structure, operation, and FET-based gas sensors

Figure 1-2 shows a typical back-gate configuration of FET device structure, which is widely used for gas sensor devices, consisting of a semiconductor as a channel, two electrodes as source and drain, and back-gate electrode.[23,24] The operation of FET device is similar to the conventional metal-oxide-semiconductor field-effect transistor (MOSFET). To establish the electric field across the dielectric layer, the gate electrode is biased. By controlling the gate voltage, the charge carrier concentration in the channel can be modulated, which affect the current flowing between the source and drain electrodes through the channel material.[25,26] This provides another option for achieving improved gas sensor performance. By measuring the conductance change of the semiconductor channel, the gas detection can be realized. That is, the changes of electronic state in the sensor device will be induced by the adsorbed gas molecules on the semiconductor surface. Additionally, sensors based on FET structure can be integrated seamlessly into the electronic circuits, which is convenient for the sensor network technology especially in the Internet-of-Things (IoT) era.[27,28] Besides, user-friendly sensor operation as well as possibility to integrate into transportable systems are another

interesting factors of FET-based gas sensors. Therefore, research developments for achieving higher gas sensor performance using FET-based structure has been kept increasing since the past few years.[19,29–31]

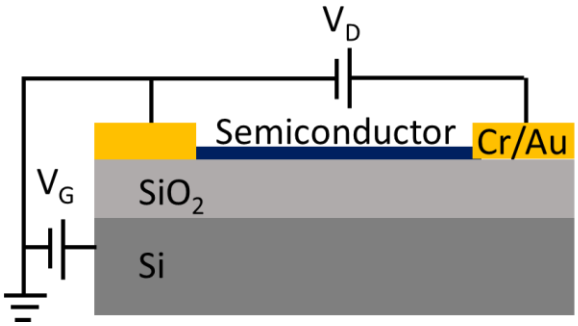

Figure 1-2. A typical back-gate configuration of FET device structure for gas sensor technology.

Typical drain current (I_D) versus drain voltage (V_D) curves with different gate voltage (V_G) for a *n*-type FET device are shown in **Figure 1-3**. Linear region of the curve can be determined at $V_D << (V_G - V_{th})$, where V_{th} is the threshold voltage, whereby I_D is linearly proportional to V_D, following Ohm's law. The properties of *I*-*V* curves in a FET are well described by the equation below:[32,33]

$$I_D = \frac{W}{L}\mu C_i[(V_G - V_{th})V_D - \frac{V_D^2}{2}^2 \qquad V_D \ll (V_G - V_{th})\text{: linear region} \qquad (1\text{-}1)$$

where *W* and *L* are width and length of semiconductor channel, respectively, μ and C_i are the carrier mobility and the capacitance of the gate insulator, respectively.

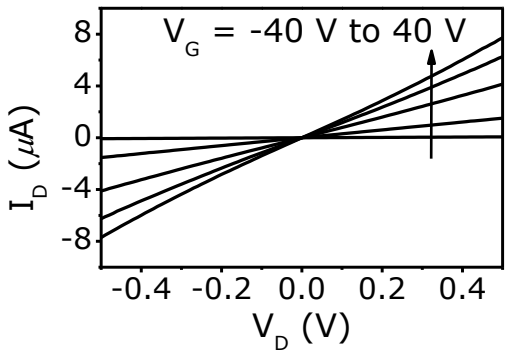

Figure 1-3. A typical current-voltage (I_D-V_D) characteristic curve of a *n*-channel FET device at different V_G gate voltage.

The sensing mechanism can be discussed as shown in **Figure 1-4** and **Figure 1-5**, which can be explored through analyzing the electron transfer process between channel material and gas molecule; the electrons are transferred to gas molecules from channel material as the gas molecule are adsorbed onto the channel material surface, resulting in the resistance increase of the gas sensor. When electrons are transferred from gas molecules to channel material, the resistance of the channel decreases. The gas response is strongly related to the electron population in the TMDC-FET, which can be further understood from the band diagram shown in **Figure 1**-5. The band diagrams illustrate the interaction of the electrons in the conduction band of TMDC with exposure of reducing gas or oxidizing gases on TMDC surface. For *n*-type channel material exposed under oxidizing gas (reducing gas), which operated under dark conditions without gate biasing as shown in **Figure 1-5a** (**Figure 1-5b**), the sensing performance is predominantly influenced by the doping effect of the gas molecule. Meanwhile, the positive gate biasing leads to the electron accumulation in TMDCs, which decreases (increases in case of reducing gas) the initial device resistance. Then, the TMDC surface attract the oxidizing gas, resulting in an increase in relative resistance changes (decrease in case of reducing case). On the other hand, the light illumination also generates electrons by photo-excitation, leading to enhancing the enhancement of relative resistance change. It can be

further improved the sensing performance by the combination of both positive gate biasing and light illumination. This cause both capacitive-induced and photoinduced electrons to accumulate for interacting with oxidizing gas (**Figure 1-5e**).

These mechanisms will be discussed in detail at each chapter for each type of gas sensor.

1.1.3. Two-dimensional (2D) materials and 2D-transition metal dichalcogenide (TMDC)-based gas sensors

Since Geim and his co-workers discovered a monolayer carbon known as graphene in 2004,[34] 2D materials field has attracted much interest around the world due to their high carrier mobility and high specific surface area.[35,36] Other than graphene, transition metal dichalcogenide (TMDC), black phosphorus (BP), metal-organic framework (MOF), and metal-oxide nanosheet (MON) have been investigated and applied in electronic devices, energy storage, optoelectronics devices, sensing applications, etc.[37–40] Besides, myriad 2D materials have been involved in gas sensing application whereby they act as a loading platform for other materials, which increasing the sensing surface area thus improving the gas sensing efficiency.[41,42] In comparison with the conventional semiconductor materials, single-layer 2D materials allow for full contact of gas molecules on the layer surface. Also, 2D materials could operate without oxygen ions, in which gas molecules can transfer electrons directly to or from 2D materials. This condition enables the sensor device for room temperature operation with low power consumption. For this reason, the introduction of 2D materials in gas sensing application could boost industrial, environmental monitoring, etc. into a higher benchmark of gas sensor development as shown in **Figure 1-6**.

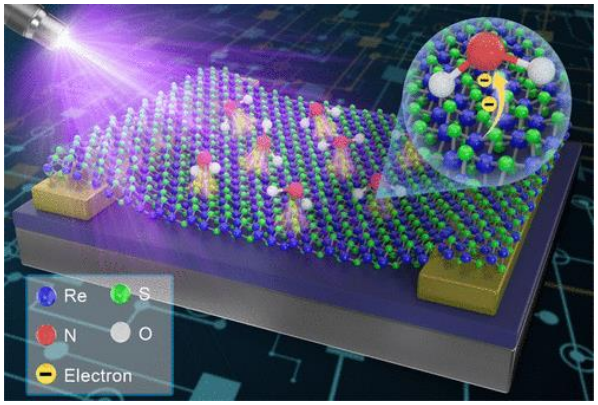

Figure 1-4. Schematic diagram of the sensing mechanism of sensor device exposed to gas molecules. (Reproduced from ref. [42], Copyright 2020, with the permission from ACS Publisher)

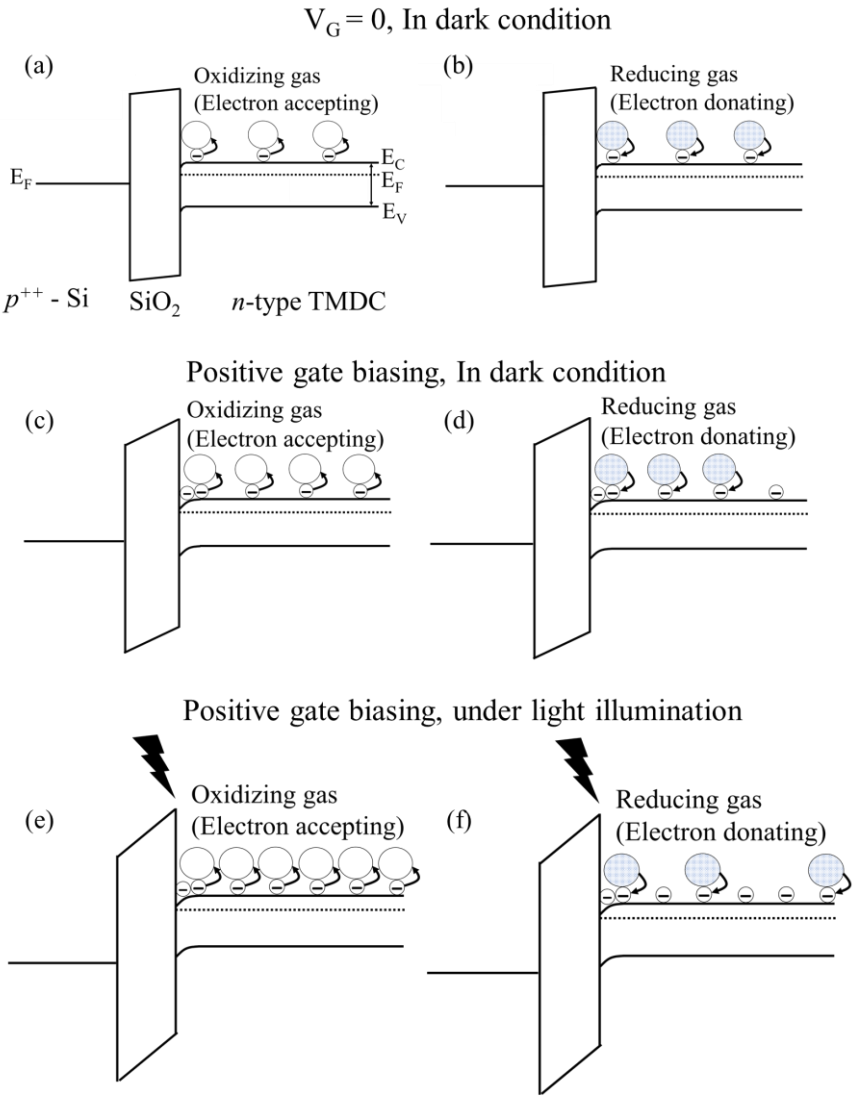

Figure 1-5. Band diagrams of the TMDC-FET, illustrating the interaction of electrons in the *n*-type TMDC with reducing gas and oxidizing gas under different sensing conditions.

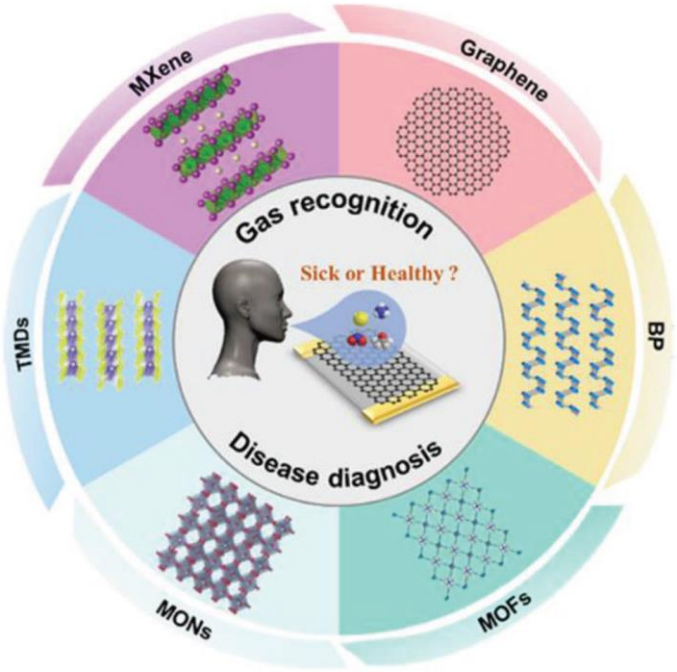

Figure 1-6. The scheme of different kinds of 2D material for industrial, exhaled breath, and environmental monitoring.

(Reproduced from ref. [43], Copyright 2019, with the permission from Wiley-VCH GmbH Publisher).

Among so many 2D materials, TMDCs are expected to be promising semiconducting materials for FET-type sensor devices. Since the last couple years, 2D-TMDCs are attracting much interest in electronic/optoelectronic applications such as transistors, photodetectors, solar cells, energy storage, sensors, etc. due to their superior semiconducting behavior and high surface-area-to-volume ratio.[23,44] TMDC is a type of MX_2 semiconductors whereby M represent transition metal atom layer (Mo, W, Re, Ti, Nb, etc.) sandwiched between two X atom layers (chalcogen atom: S, Se, Te). **Figure 1-7** shows the 2D-TMDC structure, which can be categorized into trigonal prismatic phase (hexagonal, 2H), octahedral phase (tetragonal, 1T), and their distorted phase (1T').

Among TMDC materials, molybdenum disulfide (MoS_2) and tungsten disulfide (WS_2) have been widely investigated in gas sensor applications.[45–47] In MoS_2, several S-

Mo-S layers attached with each other via weak van der Waals (vdWs) force. A bulk MoS_2 exhibits indirect bandgap of 1.2 eV while its single layer has a direct bandgap with 1.8 eV. As reported in the previous paper, MoS_2 is able to yield high response to gas molecule like O_2, NO_2, etc.[48,49] Similarly, WS_2 in bulk-form exhibits indirect bandgap with 1 eV, and its monolayer exhibits a direct bandgap of 2 eV. The gas sensing results reported in the previous report demonstrate that both H_2O and NH_3 can be physically adsorbed on WS_2 monolayer surface, whereby H_2O and NH_3 act as electron acceptor and donor, respectively[50], resulting in *n*-type and *p*-type doping effect toward WS_2. Additionally, H_2O molecules adsorbed on WS_2 layer cause negative dipole while NH_3 adsorption induces positive dipole. All of these studies suggest that 2D-TMDCs have potential sensing ability for gas sensing application.

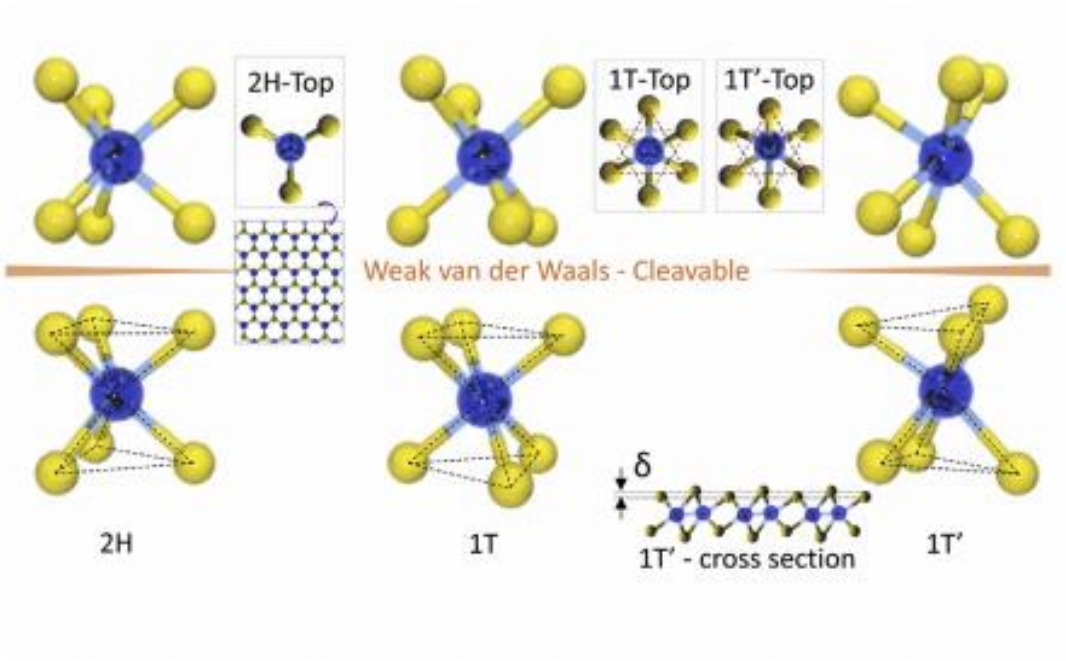

Figure 1-7. Typical structures of layered TMDCs (hexagonal 2H, tetragonal, 1T and their distorted phase 1').

(Reproduced from ref. [43], Copyright 2019, with the permission from Wiley-VCH GmbH Publisher).

1.2. Issues and challenges

Since the first concept of "gas sensor technology" proposed by Seiyama in 1962, [51] semiconductor gas sensors have been commercializing and numerous gas sensing materials have been investigated and developed such as the conventional *n*-type metal-oxides (TiO_2, SnO_2, ZnO, etc.), *p*-type metal oxides (NiO, CuO, Co_3O_4, etc.), conductive polymers (polypyrrole, polythiophene, polyaniline, etc.). Nevertheless, metal-oxide-based gas sensors operate at high temperature (>100°C) to obtain enough oxygen ions reacting with gas molecules. This condition increases the power consumption and baseline drift of the device. For comparison, conductive polymer-based gas sensors are possible to operate at room temperature. However, their gas sensing performance can be severely affected by air humidity level. In this situation, pre-treatment of dehumidification before sensing operation is inevitable, which makes the sensing procedure complicated. Additionally, over long period of storage, polymer is easily degraded, which also hinders its application. For these reasons, a broad variety of sensing materials has been investigated, and recently, a family of 2D-TMDCs, i.e. MoS_2 and WS_2 have been widely studied for gas sensing applications, which exhibited sensitive sensing operation.[14,38,52,53] Despite the importance of having a sensitive sensing material, the sensor device ability to differentiate the target gas molecule among the interfering gases is still crucial to avoid false sensor signal. In this case, device selectivity for gas detection among 2D-TMDC sensors remains a big issue especially for using a single device. For this reason, the channel surface functionalization has been examined to enhance the sensing selectivity toward a specific gas. However, the drawback of this technique is the few selections of the functionalization groups for specific target gases.[54,55] Therefore, there is an increasing requirement to explore appropriate sensing materials, device

structure, and sensing concept to acquire outstanding gas sensing performance especially enhanced selectivity using a single device. In order to address these requirements, new device concept should be developed.

As a proof of concept, new sensors for the selective and sensitive detection of humidity, oxygen, and volatile organic compound (VOC) for the environmental monitoring and industrial field will be developed. Three kinds of experiments will be conducted, which will be involved of three types of gas molecules. Firstly, the identification of humidity level is crucial in different contexts which encompass production control in agriculture, industrial and environmental monitoring, and medical diagnostics.[19] In addition, the increased demand of humidity sensing requires high response and sensitivity, and a wide detection range. Secondly, oxygen sensors are essential for a wide range of applications related to, for example, medicine, automobiles, food, and the environment. Thirdly, the long-term exposure to VOC molecules in the air has been a critical concern for both environmental and human health issues. The main reason for the severe problem in human health and animal life is the low-level exposure accumulating over long periods.

1.3. Purposes and Strategies

The purpose of this dissertation is to study the selective and sensitive detection in gas sensors based on 2D-TMDC materials FET. The selectivity and sensitivity of the sensor device will be developed to be adaptable to an on-demand detection of desired target molecules. Here, humidity, oxygen, and volatile organic compound (VOC), i.e., acetone and ethanol, are selected as the final target molecules to demonstrate the applicability of the new sensor device structure and concept for the detection of these

molecules in the environment. To achieve the goal, the sensor is developed in a few-step process. The first step is the investigation of a new channel material to be utilized in FET device structure. Here, 2D-TMDC-ReS_2 will be examined for the channel material. In the second step, the operation of ReS_2-FET transistors and photoelectrical properties are established and improved to achieve stable performance. In this step, gate biasing and light illumination with different wavelength are examined for the optimization of the sensor device's efficiency. Finally, gate-tunable and light-assisted ReS_2-FET sensor devices will be investigated for the sensor application, especially for the humidity, oxygen, and VOC gas sensors for enhancing sensitivity and selectivity performance. The details of the strategies of this study are described as following.

In this study, ReS_2 was employed as a channel material of the FET (**Figure 1-8**) among various TMDCs. It is because gate-biasing and light illumination on the 2D-TMDC devices could significantly enhance the gas sensing properties due to capacitively-induced and photo-induced carriers for interacting with gas molecules.[8–10] Nevertheless, until now, minimal research has been done to develop the gate-tunable and light-assisted sensing performance in 2D materials FET structure on gas sensing because of the limited material selection.

Semiconducting TMDCs consist of monolayers held together by weak vdW force, in which the layers are electronically and vibrationally coupled, and isolated monolayers show changes in lattice vibration energies and electronic structure as well as a transition from indirect to direct bandgap. However, there is no such variation in the ReS_2 case whereby ReS_2 in bulk-form behaves in similar manner electronically and vibrationally as monolayers. In ReS_2, the bandgap remains direct from monolayer to bulk. Also, Raman spectrum shows no dependence on the number of layers.[11] Interlayer decoupling is

further demonstrated by the insensitivity of the optical absorption to interlayer distance modulated by hydrostatic pressure. Moreover, based on the theoretical calculation, the decoupling is attributed to Peierls distortion of the 1T structure of ReS_2.[11] This prevents ordered stacking and minimizes the interlayer overlap of wavefunctions. For this reason, such vanishing interlayer coupling enables probing of two-dimensional systems without the need for monolayers. Such presented results from other previous research establish ReS_2 as an unusual, new member of the TMDCs family where the bulk acts as if it is electronically and vibrationally monolayers with the bandgap, work function, and electron affinity values of ~1.42 eV, ~4.83 eV, and ~4.30 eV, respectively. In this manner, as mentioned previously, among TMDCs, ReS_2 has attracted much attention because it has a direct bandgap matching with the visible light range regardless of thickness, unlike others TMDCs.[11,13,16,19,56,57] Therefore, ReS_2 is a promising material that overcomes the trade-off relationship between the charge carrier density with the optical absorption of thick layer and the surface-area-to-volume ratio of thin layer toward realizing a single device operation of selective and sensitive humidity, oxygen, and VOC-related gas sensors based on the effective response of ReS_2 to light illumination and gate-tunable operation.[17]

To emphasize, this study provides a device concept that focuses on the advantages of the effective drain current response of a ReS_2-FET to the light illumination to enhance the gas selectivity and sensitivity. The drain current response of the ReS_2-FET sensor to adsorbed molecules is modulated by light illumination based on different gas species. These variations for each gas molecule exhibit wavelength and carrier density dependence, allowing the sensor device to distinguish the target gas molecules from the gas mixture, thus improving sensor device selectivity.

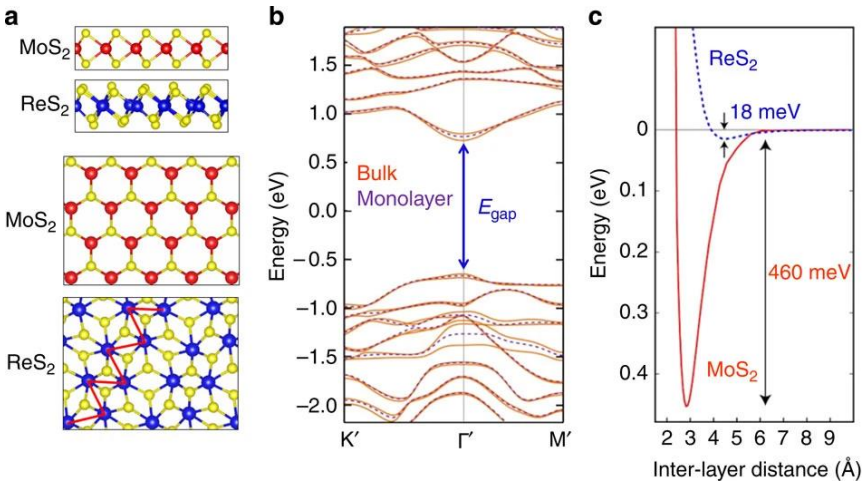

Figure 1-8. (a) Side (top two panels) and top view (bottom two panels) of ReS_2 with distorted 1T crystal structure compared with the 1H structure of conventional widely investigated TMDCs-MoS_2. (b) DFT calculated electronic band structure of bulk (orange solid curves) and monolayer (purple dashed curves) ReS_2. Both are predicted to be a direct bandgap semiconductor with nearly identical bandgap value at Γ point. (c) The calculated total energy of the system as a function of interlayer separation. The significantly shallower depth of the well in ReS_2 implies such weaker interlayer coupling energy in ReS_2 as compared with MoS_2.

(Reproduced from ref. [11], Copyright 2021, with the permission from Nature Publishing Group).

1.4. Fabrication of 2D-TMDC ReS_2-FET based gas sensors

In this section, the fabrication process of 2D-TMDC ReS_2-FET based gas sensor is described. 2D-TMDC flakes are typically produced by using the method called tape exfoliation (Scotch tape method). The exfoliated flakes are usually small in size (~5 μm), and it is usually not large enough for device fabrication.[58] Here, another method of gold-mediated exfoliation is adopted for obtaining much larger size flakes of ReS_2, which will be explained in **Section 1.4.1**. Then, the overall fabrication process of the ReS_2-FET gas sensor device will be presented in **Section 1.4.2**.

1.4.1. Gold-mediated exfoliation of large-scaled ReS_2 nanoflake

Here, gold-assisted exfoliation process of large-scale ReS_2 is explained. Gold is known to have a strong affinity for chalcogens, especially to sulfur atoms. It forms a semicovalent bond with bond strength of ~45 kcal mol^{-1}.[29,59] The interaction between gold and sulfur has been used in the formation of self-assembled monolayers of thiolated organic molecules on gold surfaces and gold-thiolate complexes. The same idea is used in this section by selectively increasing the adhesion of the topmost layer of a bulk ReS_2 crystal to gold by evaporating a thin film on it and subsequently peeling it off from the bulk crystal.

Initially, a ReS_2 crystal (HQ Graphene) was mechanically exfoliated on a thermal tape (Nitto Denko Model NO319Y-4LSC). Next, a 100 nm-thick Au film was directly deposited on an exfoliated ReS_2/thermal tape. Additional thermal tape was utilized to exfoliate the Au/ReS_2 layers from the previous ReS_2/Au coated thermal tape. Subsequently, these exfoliated Au/ReS_2 layers were pasted onto the desired target SiO_2/Si substrate before detaching the thermal tape at 100°C. All these processes and comparison of flake count for typical scotch tape exfoliated ReS_2 and gold-mediated ReS_2 can be seen in **Figure 1-9** and **Figure 1-10**, respectively.

To completely remove the residual gold layer from the ReS_2 surface, the substrate was immersed in gold etchant (AURUM-302, Kanto Chemical) for four minutes and was rinsed in deionized water for five minutes. Then, to exclude the effect of any residues that might come from this method on the gas sensing performance, an elemental analysis of gold-mediated exfoliated bulk ReS_2 was carried out by scanning electron microscopy-energy dispersive X-ray (SEM-EDX) as shown in **Figure 1-11**. The results of SEM-EDX of gold-mediated bulk ReS_2 showed that the ratio of Re:S to be 1:2. That is quantitatively

similar to the SEM-EDX data of standard bulk ReS_2. In this regard, the effect of any residues that might come from gold-mediated exfoliation process on the sensing performance was excluded. Optical microscopy images were captured using a microscope (BX51M, Olympus Co., Japan) in the reflection mode. AFM analysis was performed using Olympus/SHIMADZU Nano search microscope with a dynamic scanning probe. Raman microscopy (Nanophoton, Model: Ramanplus) was used to obtain the Raman spectra acquired under an excitation wavelength of 532 nm. These types of equipment were used to determine the crystallinity of the sample structure and film thickness, respectively. The Raman laser power on the sample was fixed at 1 mW to prevent any possible heating influence on the ReS_2 nanoflakes.

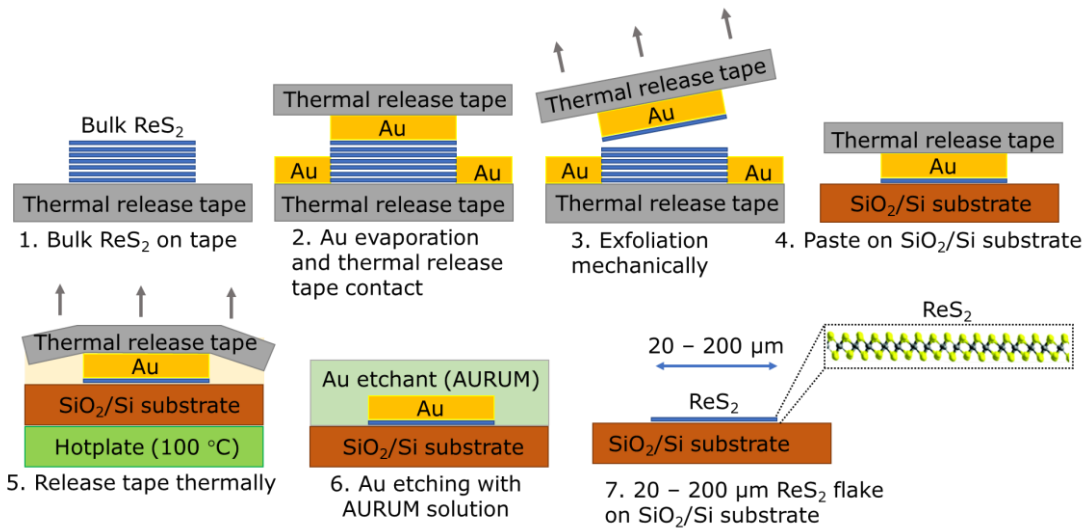

Figure 1-9. Schematic illustration of the gold-mediated exfoliation process.

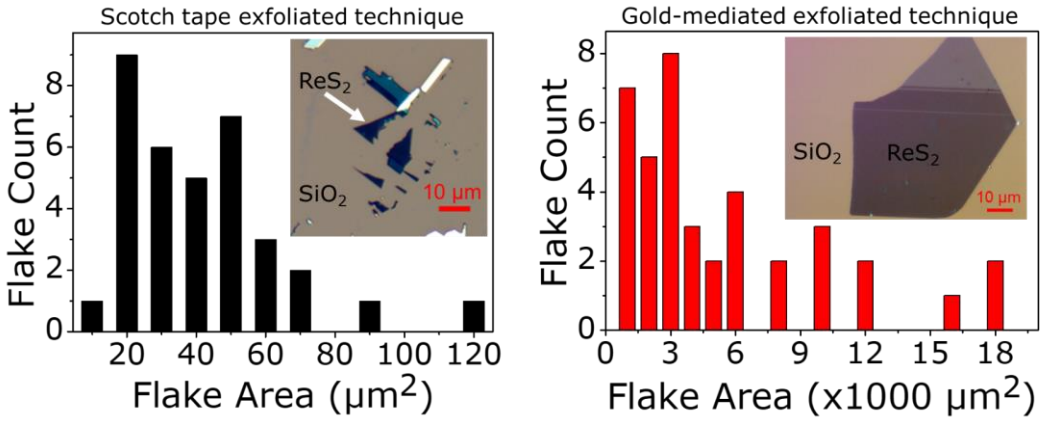

Figure 1-10. Comparison between typical scotch tape exfoliated ReS_2 and gold-mediated ReS_2 in term of flake count vs. flake area.

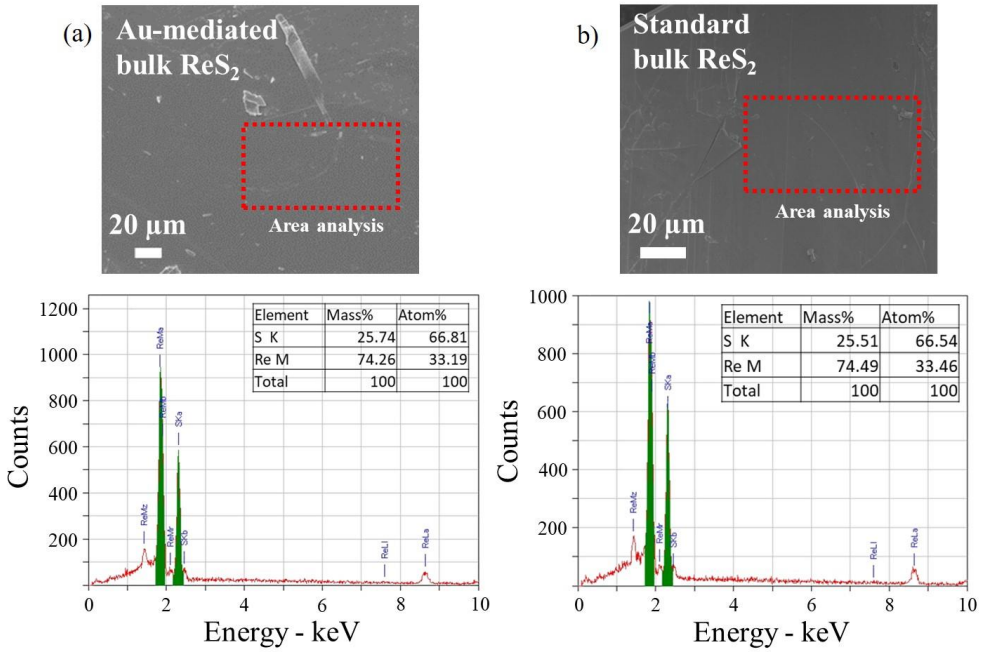

Figure 1-11. SEM image and EDX spectrum of (a) gold-mediated bulk ReS_2 and (b) standard bulk ReS_2. (Reproduced from ref. [18], Copyright 2021, with the permission from Wiley-VCH GmbH Publisher).

1.4.2. ReS_2-FET gas sensor device fabrication process

To fabricate the FET-based sensor devices, a SiO_2/Si substrate with gold-assisted exfoliated ReS_2 nanosheets was coated with a polymethyl methacrylate layer and patterned using electron-beam lithography (Elionix, ELS-7000 and ELS-F125), followed

by Cr/Au (3/80 nm) metal deposition using e-beam evaporation and a lift-off process. Here, the highly doped Si substrate and the 285 nm thick SiO_2 layer worked as a back-gate electrode and a gate dielectric layer, respectively. The sample device was then cut to form a 2.5 × 2.5 mm^2 chip using a manual scribing machine and was mounted on an eight-pin standard chip carrier using silver paste. A manual wedge bonder was utilized to realize a wire-bond connection between the chip carrier and the sensor device. The fabrication process and a photograph of the ReS_2-FET based gas sensor can be seen in **Figure 1-12**.

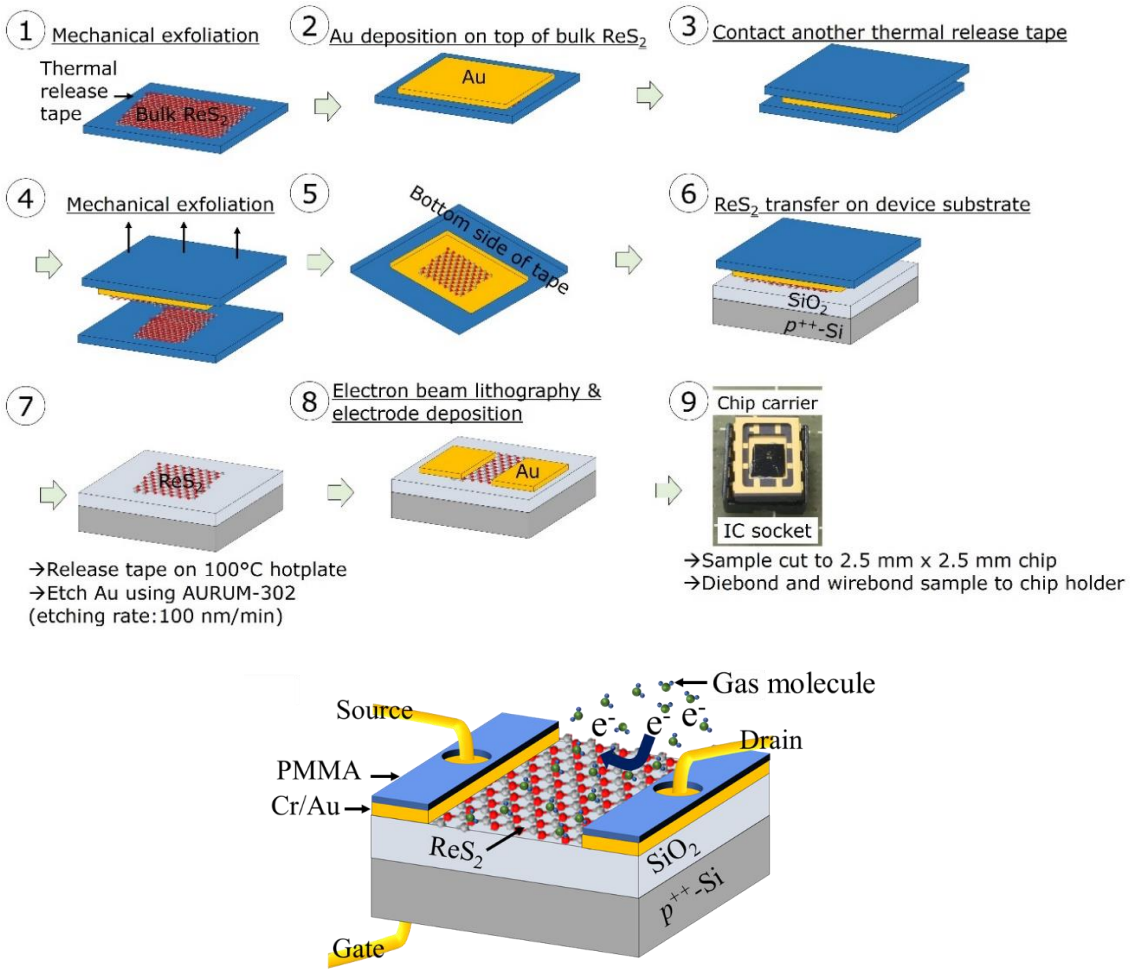

Figure 1-12. Schematic illustration of the fabrication process and a photograph of the ReS_2-FET based gas sensors.

(Reproduced from ref. [19], Copyright 2021, with the permission from IOP Publisher)

1.5. Organization

This dissertation includes five chapters. **Chapter 1** describes the general introduction, including background, problems, purposes, and approaches for this work.

In **chapter 2**, a gate biasing operation of the ReS_2-FET for humidity sensor is described. This chapter details the gate biasing operation to design the high-quality ReS_2-FET based humidity sensors. The sensing performance and underlying mechanism are discussed with respect to the gate bias operation.

Chapter 3 introduces the oxygen gas sensor performance and mechanism of few-layer-thick ReS_2-FET under both light illumination and gate biasing. The combination of light illumination and positive gate voltage enhanced the device sensing response by increasing the photogenerated carrier and charge transfer level of the ReS_2-FET.

Chapter 4 discusses the development of the detection of volatile organic compound (VOC) gases using a single device of 2D-TMDC ReS_2-FET with an enhanced selectivity by light illumination. Here, the advantages of the effective response of ReS_2 to light illumination are utilized to enhance the selectivity of gas sensing performance of a ReS_2-FET device.

Chapter 5 summarizes this dissertation.

References

[1] N. S. Bobbitt, M. L. Mendonca, A. J. Howarth, T. Islamoglu, J. T. Hupp, O. K. Farha, R. Q. Snurr, *Chem. Soc. Rev.* **2017**, *46*, 3357.

[2] E. Barea, C. Montoro, J. A. R. Navarro, *Chem. Soc. Rev.* **2014**, *43*, 5419.

[3] M. Kumar, A. V. Agrawal, R. Kumar, S. Venkatesan, A. Zakhidov, G. Yang, J. Bao, M. Kumar, *ACS Sensors* **2018**, *3*, 998.

[4] E. Wu, Y. Xie, B. Yuan, D. Hao, C. An, H. Zhang, S. Wu, X. Hu, J. Liu, D. Zhang, *ACS Appl. Mater. Interfaces* **2018**, *10*, 35664.

[5] A. W. Boots, J. J. B. N. Van Berkel, J. W. Dallinga, A. Smolinska, E. F. Wouters, F. J. Van Schooten, *J. Breath Res.* **2012**, *6*, 027108.

[6] X. Zhao, B. Cai, Q. Tang, Y. Tong, Y. Liu, *Sensors* **2014**, *14*, 13999.

[7] D. Yu, J. Li, T. Wang, X. She, Y. Sun, J. Li, L. Zhang, X. F. Yu, D. Yang, *Phys. Status Solidi - Rapid Res. Lett.* **2020**, *14*, 1.

[8] W. J. Yan, D. Y. Chen, H. R. Fuh, Y. L. Li, D. Zhang, H. Liu, G. Wu, L. Zhang, X. Ren, J. Cho, M. Choi, B. S. Chun, C. Coileáin, H. J. Xu, Z. Wang, Z. Jiang, C. R. Chang, H. C. Wu, *RSC Adv.* **2019**, *9*, 626.

[9] R. Kumar, N. Goel, M. Kumar, *ACS Sensors* **2017**, *2*, 1744.

[10] S. Yang, J. Kang, Q. Yue, J. M. D. Coey, C. Jiang, *Adv. Mater. Interfaces* **2016**, *3*, 1500707.

[11] S. Tongay, H. Sahin, C. Ko, A. Luce, W. Fan, K. Liu, J. Zhou, Y. S. Huang, C. H. Ho, J. Yan, D. F. Ogletree, S. Aloni, J. Ji, S. Li, J. Li, F. M. Peeters, J. Wu, *Nat. Commun.* **2014**, *5*, 3252.

[12] Y. C. Lin, H. P. Komsa, C. H. Yeh, T. Björkman, Z. Y. Liang, C. H. Ho, Y. S. Huang, P. W. Chiu, A. V. Krasheninnikov, K. Suenaga, *ACS Nano* **2015**.

[13] B. Mukherjee, A. Zulkefli, R. Hayakawa, Y. Wakayama, S. Nakaharai, *ACS Photonics* **2019**, *6*, 2277.

[14] M. Rahman, K. Davey, S. Z. Qiao, *Adv. Funct. Mater.* **2017**, *27*, 1606129.

[15] G. Nazir, M. A. Rehman, M. F. Khan, G. Dastgeer, S. Aftab, A. M. Afzal, Y. Seo, J. Eom, *ACS Appl. Mater. Interfaces* **2018**, *10*, 32501.

[16] Y. Xiong, H. W. Chen, D. W. Zhang, P. Zhou, *Phys. Status Solidi - Rapid Res. Lett.* **2019**, *13*, 1.

[17] B. Mukherjee, A. Zulkefli, K. Watanabe, T. Taniguchi, Y. Wakayama, S. Nakaharai, *Adv. Funct. Mater.* **2020**, 2001688.

[18] A. Zulkefli, B. Mukherjee, R. Hayakawa, T. Iwasaki, S. Nakaharai, Y. Wakayama, *Phys. Status Solidi - Rapid Res. Lett.* **2020**, pssr. 202000330.

[19] A. Zulkefli, B. Mukherjee, T. Iwasaki, R. Hayakawa, S. Nakaharai, Y. Wakayama, *Jpn. J. Appl. Phys.* **2021**, *60*, SBBH01.

[20] Y. F. Sun, S. B. Liu, F. L. Meng, J. Y. Liu, Z. Jin, L. T. Kong, J. H. Liu, *Sensors* **2012**, *12*, 2610.

[21] V. Dobrokhotov, A. Larin, *ChemEngineering* **2019**, *3*, 1.

[22] T. Jarvinen, G. S. Lorite, J. Perantie, G. Toth, S. Saarakkala, V. K. Virtanen, K. Kordas, *Nanotechnology* **2019**, *30*, 405501.

[23] D. Jariwala, V. K. Sangwan, L. J. Lauhon, T. J. Marks, M. C. Hersam, *ACS Nano* **2014**, *8*, 1102.

[24] R. Vargas-bernal, **2019**, 100.

[25] J. K. Huang, J. Pu, C. L. Hsu, M. H. Chiu, Z. Y. Juang, Y. H. Chang, W. H. Chang, Y. Iwasa, T. Takenobu, L. J. Li, *ACS Nano* **2014**, *8*, 923.

[26] W. Liao, W. Wei, Y. Tong, W. K. Chim, C. Zhu, *ACS Appl. Mater. Interfaces* **2018**,

10, 7248.

[27] M. T. Lazarescu, *IEEE J. Emerg. Sel. Top. Circuits Syst.* **2013**, *3*, 45.

[28] S. D. T. Kelly, N. K. Suryadevara, S. C. Mukhopadhyay, *IEEE Sens. J.* **2013**, *13*, 3846.

[29] M. A. Zulkefli, B. Mukherjee, R. Hayakawa, T. Iwasaki, S. Nakaharai, Y. Wakayama, *Phys. Status Solidi - Rapid Res. Lett.* **2020**, 2000330.

[30] J. Kim, H. Yoo, H. O. Choi, H. Jung, *Nano Lett.* **2014**, *14*, 5941.

[31] D. J. Late, Y. K. Huang, B. Liu, J. Acharya, S. N. Shirodkar, J. Luo, A. Yan, D. Charles, U. V. Waghmare, V. P. Dravid, C. N. R. Rao, *ACS Nano* **2013**, *7*, 4879.

[32] G. Horowitz, *Adv. Mater.* **1998**, *10*, 365.

[33] L. Torsi, M. Magliulo, K. Manoli, G. Palazzo, *Chem. Soc. Rev.* **2013**, *42*, 8612.

[34] K. S. Novoselov, A. K. Geim, *Science (80-.).* **2004**, *306*, 666.

[35] F. Schedin, A. K. Geim, S. V. Morozov, E. W. Hill, P. Blake, M. I. Katsnelson, K. S. Novoselov, *Nat. Mater.* **2007**, *6*, 652.

[36] P. Taylor, S. Das, M. Kim, J. Lee, W. Choi, S. Das, M. Kim, J. Lee, W. Choi, *Crit. Rev. Solid State Mater. Sci.* **2014**, *34*, 231.

[37] Q. H. Wang, K. Kalantar-Zadeh, A. Kis, J. N. Coleman, M. S. Strano, *Nat. Nanotechnol.* **2012**, *7*, 699.

[38] W. Yang, L. Gan, H. Li, T. Zhai, *Inorg. Chem. Front.* **2016**, *3*, 433.

[39] S. Cho, B. Anasori, C. Kim, Y. Choi, J. Kim, Y. Gogotsi, *ACS Nano* **2018**, *12*, 986.

[40] Z. Gu, W. Song, Z. Yang, R. Zhou, *Phys. Chem. Chem. Phys.* **2018**, *20*, 30384.

[41] Y. Zhou, *J. Mater. Chem. A* **2018**, *6*, 10286.

[42] J. Zeng, Y. Niu, Y. Gong, Q. Wang, H. Li, A. Umar, N. F. de Rooij, G. Zhou, Y. Wang, *ACS sensors* **2020**, *5*, 3172.

[43] L. Zhang, K. Khan, J. Zou, H. Zhang, Y. Li, *Adv. Mater. Interfaces* **2019**, *6*, 1901329.

[44] D. Akinwande, C. Huyghebaert, C. H. Wang, M. I. Serna, S. Goossens, L. J. Li, H. S. P. Wong, F. H. L. Koppens, *Nature* **2019**, *573*, 507.

[45] A. Venkatesan, S. Rathi, I. Y. Lee, J. Park, D. Lim, M. Kang, H. I. Joh, G. H. Kim, E. S. Kannan, *Nanotechnology* **2017**, *28*, 365501.

[46] S. Y. Choi, Y. Kim, H. S. Chung, A. R. Kim, J. D. Kwon, J. Park, Y. L. Kim, S. H. Kwon, M. G. Hahm, B. Cho, *ACS Appl. Mater. Interfaces* **2017**, *9*, 3817.

[47] D. H. Youn, B. J. Kim, S. J. Yun, *Nanotechnology* **2020**, *31*, 105602.

[48] S. Zhao, J. Xue, W. Kang, *Chem. Phys. Lett.* **2014**, *595–596*, 35.

[49] A. Shokri, N. Salami, *Sensors Actuators, B Chem.* **2016**, *236*, 378.

[50] C. J. Zhou, W. H. Yang, Y. P. Wu, W. Lin, H. L. Zhu, *J. Phys. D. Appl. Phys.* **2015**, *48*, 285303.

[51] T. Seiyama, A. Kato, K. Fujiishi, M. Nagatani, *Anal. Chem.* **1962**, *34*, 1502.

[52] D. J. Late, B. Liu, H. S. S. R. Matte, V. P. Dravid, C. N. R. Rao, *ACS Nano* **2012**, *6*, 5635.

[53] T. Pham, G. Li, E. Bekyarova, M. E. Itkis, A. Mulchandani, *ACS Nano* **2019**, *13*, 3196.

[54] J. Kim, H. Yoo, H. O. Choi, H. Jung, *Nano Lett.* **2014**, *14*, 5941.

[55] S.-Y. Cho, H.-J. Koh, H.-W. Yoo, J.-S. Kim, H.-T. Jung, *ACS Sensors* **2017**, *2*, 183.

[56] P. Nagler, G. Plechinger, C. Schüller, T. Korn, *Phys. Status Solidi - Rapid Res. Lett.* **2016**, *10*, 185.

[57] J. M. Urban, M. Baranowski, A. Kuc, L. Klopotowski, A. Surrente, Y. Ma, D.

Wlodarczyk, A. Suchocki, D. Ovchinnikov, T. Heine, D. K. Maude, A. Kis, P. Plochocka, *2D Mater.* **2019**, *6*, 015012.

[58] M. Tosun, S. Chuang, H. Fang, A. B. Sachid, M. Hettick, Y. Lin, Y. Zeng, A. Javey, *ACS Nano* **2014**, *8*, 4948.

[59] S. B. Desai, S. R. Madhvapathy, M. Amani, D. Kiriya, M. Hettick, M. Tosun, Y. Zhou, M. Dubey, J. W. Ager, D. Chrzan, A. Javey, *Adv. Mater.* **2016**, *28*, 4053.

[60] L. D. Bharatula, M. B. Erande, I. S. Mulla, C. S. Rout, D. J. Late, *RSC Adv.* **2016**, *6*, 105421.

Chapter 2

Gate-Bias Tunable Humidity Sensors Based on Rhenium Disulfide Field-Effect Transistors

Chapter 2 reports about gate-bias tunable humidity sensors based on rhenium disulfide field-effect transistors. It is divided into several sections, namely introduction, experimental, results and discussions, conclusion, and supplementary data. The experimental section is divided into sub-section namely gas sensing measurement of ReS_2-FET based humidity sensor. Meanwhile, the section of results and discussions section is divided into sub-sections of structural characterization, electrical and sensing properties, and response-recovery time, reversibility and stability properties. The section of supplementary data is divided into control study of ReS_2 thickness on humidity sensing performance. The details for each section are described as below.

2.1. Introduction

Humidity measurement is important in industry and environmental monitoring. Relative humidity (RH) monitoring is widely used in gas detection, electronic dry cabinet, clean room, cryogenic processes, human comfort, etc. The most common RH sensing methods use changes in resistance, capacitance, thermal conductivity, and others. Considerable work to enhance the gas sensor has been reported ranging from heterostructure, intentional plasma-induced detected material, and surface functionalization.[1,2] However, the investigation of humidity sensing performance and mechanism based on gate-bias effect, especially gas-solid interaction have not yet been

explored. In this manner, it would be fascinating to examine the humidity sensor under gate-bias effect for further progress of high-performance humidity sensor.

In this chapter, ReS_2-FET based humidity sensors was investigated. The sensing performance including response, sensitivity, response-recovery time, reversibility, and stability were examined in an orderly approach. This chapter focuses on the gate voltage operation to explain their functions in the sensing mechanism. In consequence, high sensing response was achieved especially in low relative humidity (RH) range by utilizing the negative gate bias effect. Sensing response based on the threshold voltage change was discovered to be a superior sensing parameter for a broad RH range monitoring, together with high response and sensitivity. A practical sensitivity of 0.4 V per 1% RH was attained. This chapter aims to provide a thorough understanding of the functions of gate biasing, contributing to the development of a high-quality humidity sensor based on ReS_2-FET.

2.2. Experimental

2.2.1. Sensing measurement of ReS_2-FET based humidity sensor

The RH level was regulated by altering the ratio of dry and wet air by utilizing a mixing connector connected to mass flow controllers, which are prepared in the home-built gas measurement setup as demonstrated in **Figure 2-1**. The gas chamber dimensions are 2.5 cm × 6.0 cm × 9.0 cm. A total flow rate of 1 L/min was incorporated for dry and wet air. The gas chamber was flushed with pure nitrogen gas for several minutes to ensure the sensor returns to its original state after every measurement. A source-measurement unit (Keysight B2912A) was employed to assess the sensing and electrical properties. All

measurements were carried out at room temperature, which were maintained with a temperature-controlled heater underneath the gas chamber.

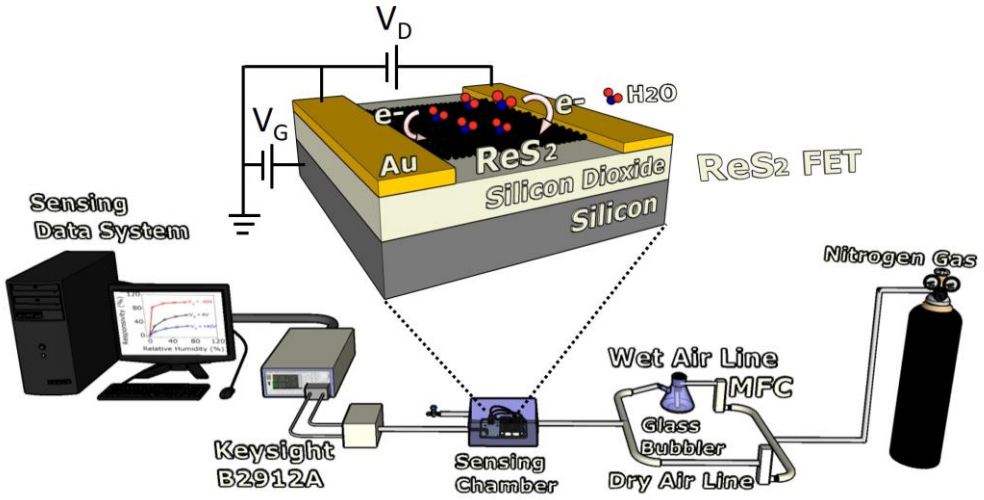

Figure 2-1. Schematic illustration of the home-built gas sensing measurement setup and the ReS_2-FET based humidity sensor.

(Reproduced from ref. [3], Copyright 2021, with the permission from IOP Publisher).

2.3. Results and discussion

2.3.1. Structural characterization

Figures 2-2a and **2-2**b illustrate an AFM image and the height profile (green line in the AFM image) of the ReS_2 nanoflake, correspondingly. The height is approximately 8 nm, corresponding to 11-layer-thick ReS_2 (See **Figure S2-1**, section of supplementary data in this chapter for the study of the thickness-dependent on humidity sensing properties). **Figure 2-2**c shows a Raman spectrum of the ReS_2 nanoflake obtained at the location by the red circle shown in the inset optical image. Within the range of 100–450 cm^{-1} Raman shift, 18 first-order modes were observed. Each Raman peak is of A_g symmetry.[4,5] A_g^1, A_g^2, and A_g^3 near 150 cm^{-1}, 437 cm^{-1} and 418 cm^{-1} are the in-plane, out-of-plane, and quasi-out-of-plane modes, respectively. This finding established the elevated chemical purity and crystallinity of the ReS_2 nanoflake. [4,5]

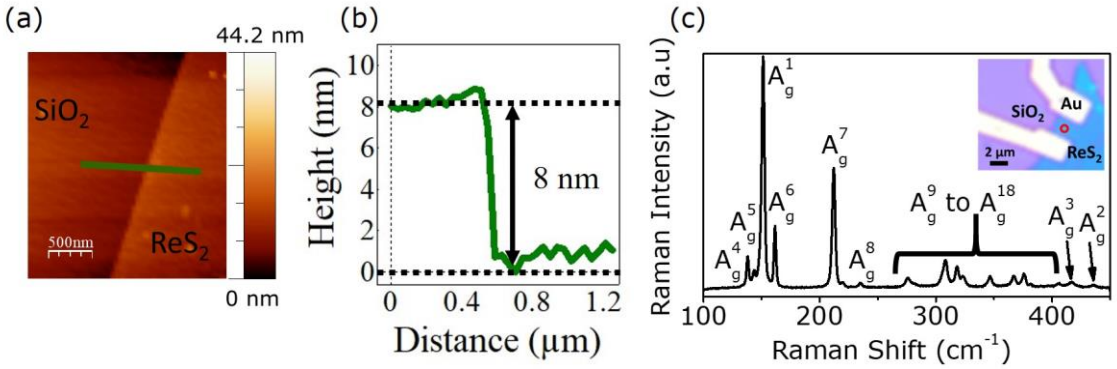

Figure 2-2. (a) AFM image, (b) AFM height profile and (c) Raman spectrum of 11 layers ReS_2 nanoflake acquired at the location by the red circle shown in the inset optical image.

(Reproduced from ref. [3], Copyright 2021, with the permission from IOP Publisher).

2.3.2. Electrical and sensing properties

As a reference, the typical output and transfer curves of the ReS_2-FET at 0% RH was initially measured as shown in **Figure 2-3**a and **2-3**b, respectively. The linear curves in **Figure 2-3**a indicate ohmic contacts between electrodes and the ReS_2 channel. The typical *n*-type operation in **Figure 2-3**b implies electrons as majority carriers in the ReS_2-FET, in which the origin of *n*-type ReS_2 material is determined by the carrier injection of electron. The measured mobility and the ON-OFF current ratio of the ReS_2-FET were ca. 24 $cm^2\ V^{-1}\ s^{-1}$ and ca. 10^5, respectively at a source-drain voltage (V_D) of 1 V (see **Figure S2-2**, section of supplementary data in this chapter). Then, the humidity sensing behavior of an ReS_2-FET was examined. **Figure 2-3**c shows the output curves of the ReS_2-FET without a gate voltage (V_G = 0). These curves were measured in a 0% to 70% RH range. As seen in **Figure 2-3**c, the drain current gradually rises as the RH level increased, which caused by the feature of the water molecule as an electron donor[6], i.e., electrons were transferred from the physically adsorbed water molecules into the ReS_2 channel to stimulate the device resistance changes. The sensing response as a function of RHs is

shown in **Figure 2-3**d (black line). Initially, this was calculated as the relative resistance change ($\frac{\Delta R}{R_{N_2}}$) according to the following Equation:

$$\frac{\Delta R}{R_{N_2}} = \left[\frac{R_{N_2} - R_{H_2O}}{R_{N_2}} \times 100\right]\% \qquad (2-1)$$

where R_{H_2O} and R_{N_2} refer to the channel resistances in humid vapour and nitrogen gas (RH = 0), correspondingly (Nitrogen has been chosen as a background gas because nitrogen does not have any impact onto the transistor properties as shown in supplementary data sub-chapter 2.5). The response increased monotonically with increasing RH. Importantly, it changes greatly from 0% to 40% in the low RH range (0–20%). Meanwhile, a relatively small change from 56 to 60% was observed in the high RH range (50–70%). This minor change can be attributed to the coverage of the water molecules on the ReS_2 channel surface (water molecule is fully cover on the channel surface) that represses the electron doping from the adsorbed water molecules into ReS_2.

This tendency was changed significantly by gate biasing as shown in **Figure 2-3**d (red and blue line). This was measured from 0–70% RH range. Importantly, the negative gate voltage reduced the drain current and greatly enhanced the response at the low RH range. However, this high negative gate voltage also had an impact on sensing response; it was saturated above 20% RH. As a result, the ReS_2 surface was fully covered immediately even at a low RH, and further electron doping was reduced at a high RH. This is opposed to a positive gate voltage operation, which reduced the sensing response. This occurrence can be comprehended based on the band diagrams visualised in **Figure 2-4**. The electrons interaction is demonstrated in the conduction band of ReS_2 with the

water molecules on the ReS_2 surface. **Figure 2-4**a depicted that the response is primarily influenced by the doping effect of the water molecules under thermal equilibrium (V_G = 0). Meanwhile, under the positive gate biasing, the electrons accumulated in ReS_2, which decreases R_{N_2} as shown in **Figure 2-4**b. For this case, the ReS_2 surface repel the water molecules, resulting in a decrease in ΔR. Thus, the response is reduced. **Figure 2-4**c illustrates that the negative gate biasing particularly contributes to electron depletion in ReS_2, which enhanced R_{N_2}. Subsequently, the ReS_2 surface engages the water molecules which contributes to an increased in ΔR. As a result, the response is enhanced. These results demonstrate the tunability of sensing response by controlling the gate voltage. Specifically, a negative gate voltage is advantageous for detecting low-level RH. However, the non-linearity of the response-RH curves in **Figure 2-3**d (blue line) is disadvantageous for wide range sensing. Meanwhile, a positive gate voltage is advantageous for linearity detection, but its sensing response is low.

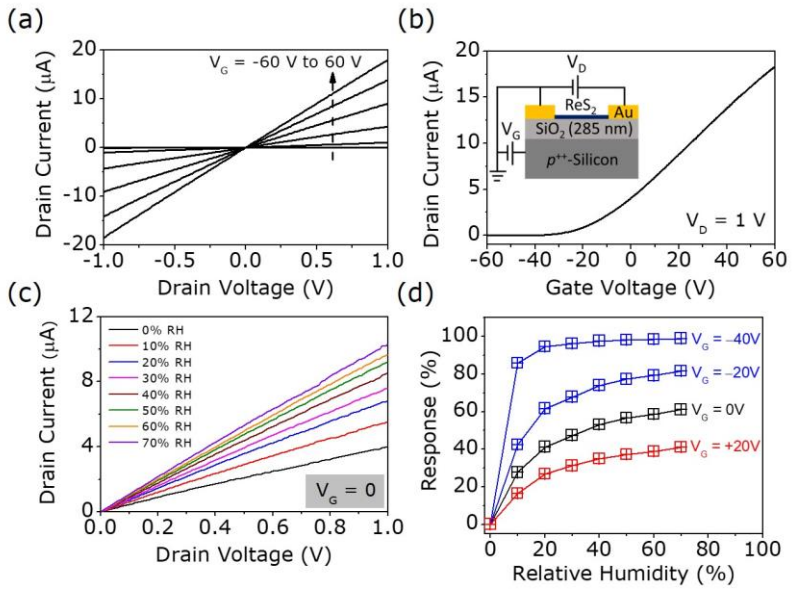

Figure 2-3. (a) The typical output and (b) transfer characteristics of the 11 layers ReS_2-FET at 0%RH. (c) Output characteristics under different RHs and (d) Response vs. RH curves of the ReS_2-FET with different gate voltages.

(Reproduced from ref. [3], Copyright 2021, with the permission from IOP Publisher).

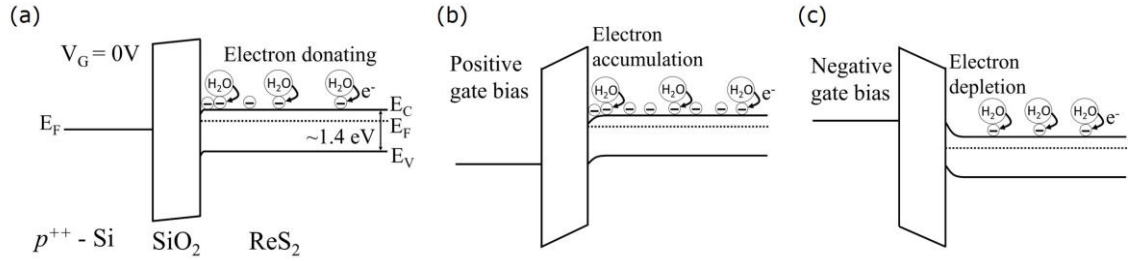

Figure 2-4. Band diagram of the ReS_2-FET, showing the electrons interaction in ReS_2 with water molecules measured at a (a) zero, (b) positive, and (c) negative gate biasing.

(Reproduced from ref. [3], Copyright 2021, with the permission from IOP Publisher).

In contrast, the sensing response based on threshold voltage changes (ΔV_{th}) is observed to exhibit a continuous variation against RH over a wide range sensing up to 70% RH as shown in **Figure 2-5**a and **Figure 2-5**b. Here, the ΔV_{th} is the difference between the threshold voltage at 0% RH ($V_{th,dry}$) and those obtained at a range of humidity values ($V_{th,humid,}$). The ΔV_{th} varied from 0 V to 32 V as RH was increased from 0% to 70%. From **Figure 2-5**c, the sensing sensitivity based on ΔV_{th} was obtained from the line slope between the ΔV_{th} and RHs by using the following equation:

$$S_{O_2} = \left[\frac{\partial\,(\Delta V_{\mathrm{th}})}{\partial \mathrm{RH}}\right] \qquad (2-2)$$

The sensing sensitivity of 0.4 V per 1% RH was achieved. This emphasises that the humidity sensing performance in this chapter study is significantly remarkable among the described humidity sensors (**Table 2-1**) by utilizing the ΔV_{th} as a superior sensing parameter.

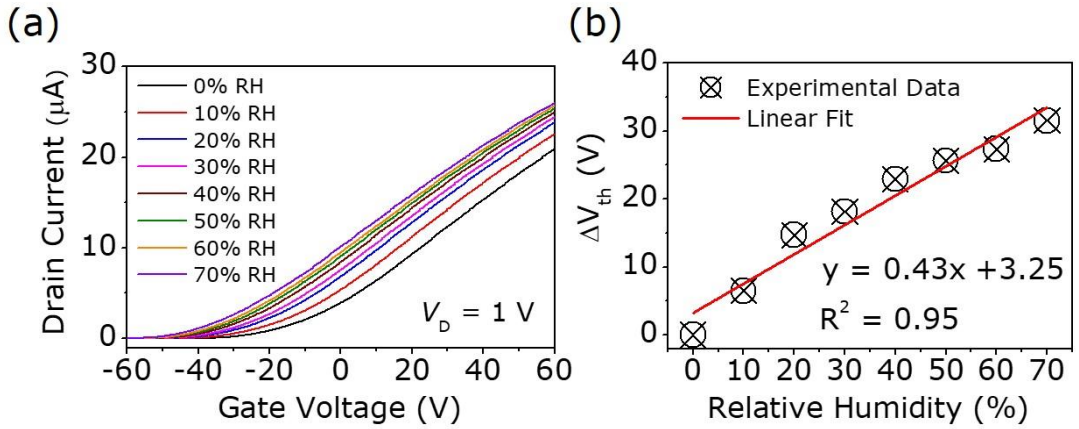

Figure 2-5. (a) Transfer characteristics of the ReS_2-FET with different RHs in linear scale. (b) Response in terms of threshold voltage change ($\Delta V_{th} = V_{th,dry} - V_{th,humid}$) dependence on RH.

(Reproduced from ref. [3], Copyright 2021, with the permission from IOP Publisher).

Table 2-1. Comparison of humidity sensors of various nanomaterials.

Sensing material	Type of sensor	Response	Sensitivity	Response/recovery time (s)	[Ref.] Year
SnO_2	Transistor	3500% ($\Delta I_{RH}/I_{dry}$)	–	120–170/20–60	[7] 2007
ZnO	Piezoelectricity	–	14 kHz/%RH	25/25	[8] 2010
Carbon nanotube	Capacitance	–	35.86%/%RH ($\Delta C/\Delta$ %RH)	75/140	[9] 2011
GO	QCM-type	–	22.1 Hz/%RH	12/18	[10] 2011
MoS_2	Transistor	800% ($\Delta R/R$)	–	300/600	[11] 2013
GO, ZnO	SAW	–	53kHz/%RH	1/19	[12] 2014
Graphene	Resistance	35% ($\Delta R/R$)	–	108/94	[13] 2014
GO	Optics	–	55.3 (dB/%RH)	0.67/0.67	[14] 2014
V_2O_5	Resistance	45.3% ($\Delta R/R$)	–	240/300	[15] 2015

Black phosphorus	Resistance	97% ($\Delta R/R$)		360/10	[16] 2016
GO	Resistive	–	0.14 mV/%RH	189±49/89±5	[17] 2016
γ-Al_2O_3	Capacitance	9.378 (pF/RH)	–	150/52	[18] 2016
Black phosphorus	Transistor	521% ($\Delta R/R$)	–	101/26	[19] 2016
CVD ReS_2	Resistive	–60% ($\Delta R/R_d$)	–	20/10	[20] 2016
Graphene/Si Schottky junction	Resistance & reverse biased	–	45%/RH ($\Delta I/I\Delta$%RH)	8/19	[21] 2017
MPA/c-ReS_2	Transistor	80% ($\Delta G/G_{inert}$)	–	4.1/1	[1] 2019
gold-assisted exfoliated ReS_2	Resistive & gate-bias effect	98.9% ($R_{N_2}-R_{H_2O}/R_{N_2}$)	0.4 V/%RH (ΔV_{th}/%RH)	30/50	This work

(Reproduced from ref. [3], Copyright 2021, with the permission from IOP Publisher).

2.3.3. Response-recovery time, reversibility, and stability properties

The response and recovery time characteristics were investigated as shown in **Fig. 2-6**a. These measurements were conducted at V_G = –20 V and V_D = 1 V from the initial state 40% RH. Next, 70% RH water vapour was added into the sensing chamber before decreasing again to 40% RH. The response and recovery time were expressed as the time needed for a sensor to achieve 90% of its steady response and back to 10% of the value, correspondingly.[22,23] The response and recovery time were individually extricated at 30 and 50 seconds, correspondingly. The duration was quicker compared to most of the described humidity sensors according to numerous nanomaterials (**Table 2-1**).

The reversibility of the sensor performance against humidity was also conducted out. **Figure 2-6**b shows a Raman spectrum of the ReS_2 nanoflake under 40% (red line) and 70% (blue line) RH. As increasing RH from 40% to 70%, the Raman peaks of A_g^1, A_g^6, and A_g^7 were slightly shifted to high energy of 0.382 cm^{-1}, 0.765 cm^{-1}, and 0.755 cm^{-1}, correspondingly. These shifted peaks result from the electrons doping caused by the change in the electron-phonon interactions. This result supports the above discussion and agrees with previous reports, in which gas or water molecules with electron-donating or withdrawing capabilities induce a charge transfer for sensing.[24,25] Subsequently, the peaks returned to their original positions as decreasing RH from 70% to 40% (black line). This indicates that the adsorption and desorption of water molecules were induced and accorded well with the increase and decrease in RHs. To examine the stability, the sensing measurements were repeated after one month. As shown in **Fig. 2-6**c**)**, the response is majorly unchanged even after one-month period, indicating that the device has long-term stability and durability. The outcomes indicate the sensor's strong potential to be used in real-time applications.

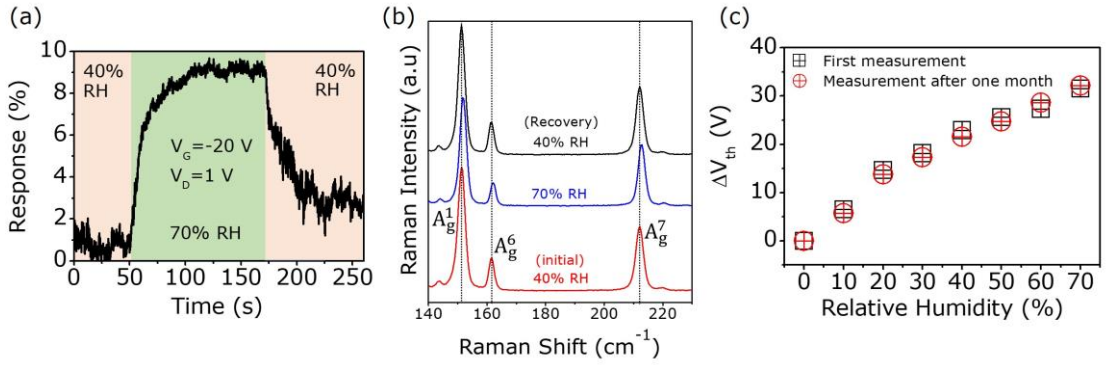

Figure 2-6. (a) Analysis of response time extracted from one cycle of RHs variation from 40% to 70% and back to 40%. (b) Raman peaks of $\mathbf{A_g^1}$, $\mathbf{A_g^6}$, and $\mathbf{A_g^7}$ modes, showing reversible shifts in accordance with the humidity increase-decrease cycle. (c) ΔV_{th}-RH curves, proving long-term stability for humidity sensing even after one-month measurement.

(Reproduced from ref. [3], Copyright 2021, with the permission from IOP Publisher).

2.4. Conclusion

This chapter employed gate biasing operation to design high-quality ReS_2-FET based humidity sensors. The sensing performance and underlying mechanism were discussed with respect to the gate bias operation. Negative gate biasing enhanced the sensing response by decreasing the doping level of the ReS_2-FET especially in the low humidity range. Importantly, threshold voltage change was found to be the superior sensing parameter for a linearity, wide RH range monitoring with high response and sensitivity. A practical sensitivity of 0.4 V per 1% RH was attained which surpassed the results reported in prior research. Moreover, long-term stability and reversibility operations actualised the utilization of the sensor in real-time applications with quick response and recovery time. The findings indicate that a gate-bias-tunable humidity sensor based on an ReS_2-FET possesses the competency to promote more advanced sensor development towards adaptable tunable humidity sensors. Future studies are yet to be considered for further understanding on gas sensing properties of ReS_2-FET device. This including the gas flow rate dependence study on gas sensing performance.

2.5. Supplementary data

2.5.1. Control study of ReS_2 thickness on humidity sensing response

3-, 11-, and 15-layer ReS_2-FETs were prepared to explain the effect of the ReS_2 thickness on humidity sensing response. **Figure S2-1** shows the response of each sensor under various relative humidity (RH) changing from 0 to 70%. This was operated under –40 V gate bias. The sensing response increased for decreasing thicknesses between 15 layers and 11 layers ReS_2, and decreased for decreasing thicknesses between 11 layers and 3 layers ReS_2. The results could be interpreted in terms of carriers conduction at the SiO_2/ReS_2 interface and carriers exchange between adsorbed gaseous and ReS_2 surface.

For 15 layers thick ReS_2, the sensing response decrease could be due to lower surface-area-to volume ratio which reduce the gas adsorption. Thus, the carriers exchange between adsorbed gas and ReS_2 was reduced. For 3 layers thick ReS_2, the sensing response decrease. This could be explained by the fully depleted channel layer under –40 V gate bias, which increased the channel resistance. Thus, the device is in a fully OFF state and there is no carrier conduction at the SiO_2/ReS_2 interface. In this regards, 11 layers thick ReS_2 fulfilled the balance between both effects on the sensing response, i.e. the carriers conduction at the SiO_2/ReS_2 interface and carriers exchange between adsorbed gaseous and ReS_2 surface.

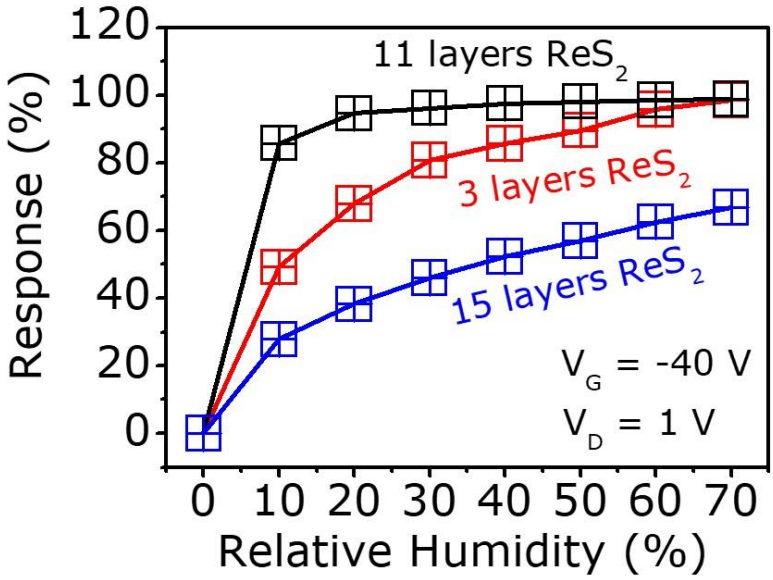

Figure S2-1. Response vs. RH curves for 3-, 11-, and 15-layer ReS_2-FETs.
(Reproduced from ref. [3], Copyright 2021, with the permission from IOP Publisher).

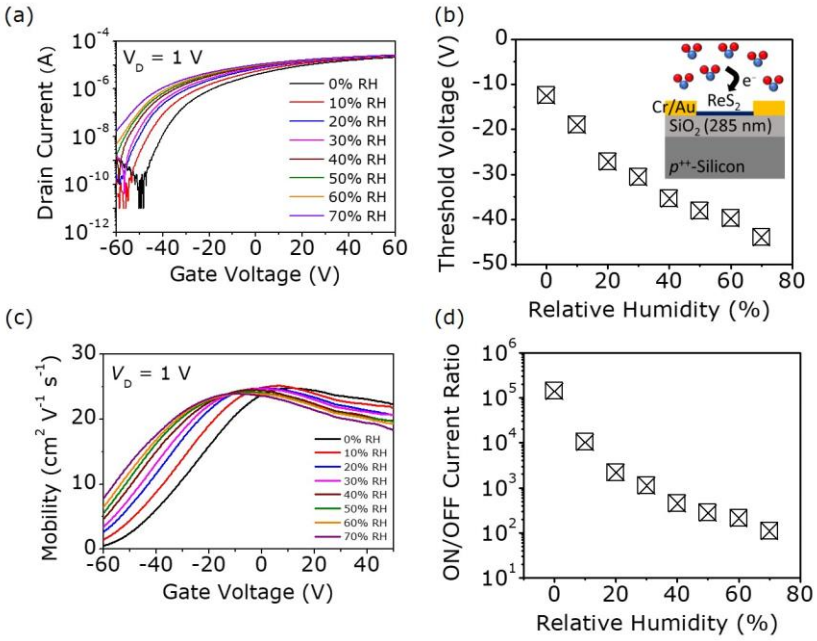

Figure S2-2. (a) Transfer characteristics of the ReS_2-FET with different RHs in semi-log scale. (b) Threshold voltages shift to negative direction with increased RHs due to the enhanced doping level by physically adsorbed water molecules. (c) Field-effect mobilities, and (d) the ON-OFF current ratios that decreases upon RH increments.

(Reproduced from ref. [3], Copyright 2021, with the permission from IOP Publisher).

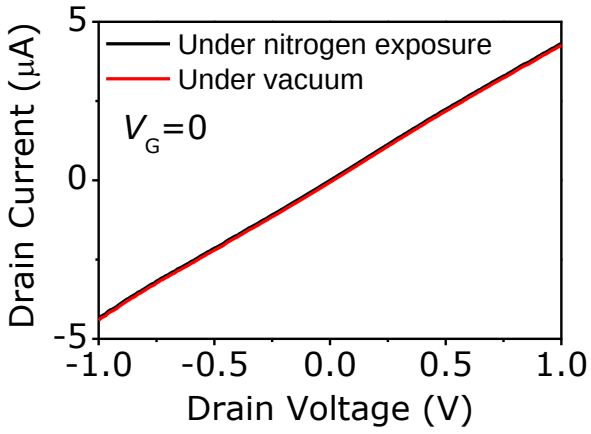

Figure S2-3. (a) Drain current vs. drain voltage characteristics of the ReS_2-FET at 0%RH (under nitrogen exposure) and under vacuum condition. The result shows that nitrogen does not have an impact on transistor properties. That is why nitrogen was picked up as a background gas.

(The content in this chapter is reproduced from [3], Copyright 2021, with permission from IOP Publisher)

References

[1] B. Martín-garcía, D. Spirito, S. Bellani, M. Prato, V. Romano, A. Polovitsyn, R. Brescia, R. Oropesa-nuñez, L. Najafi, A. Ansaldo, G. D. Angelo, V. Pellegrini, R. Krahne, I. Moreels, F. Bonaccorso, Small 2019, 15, 1904670.

[2] S. Yang, J. Kang, Q. Yue, J. M. D. Coey, C. Jiang, Adv. Mater. Interfaces 2016, 3, 1500707.

[3] A. Zulkefli, B. Mukherjee, T. Iwasaki, R. Hayakawa, S. Nakaharai, Y. Wakayama, Jpn. J. Appl. Phys. 2021, 60, SBBH01.

[4] N. R. Pradhan, A. McCreary, D. Rhodes, Z. Lu, S. Feng, E. Manousakis, D. Smirnov, R. Namburu, M. Dubey, A. R. Hight Walker, H. Terrones, M. Terrones, V. Dobrosavljevic, L. Balicas, Nano Lett. 2015, 15, 8377.

[5] A. McCreary, J. R. Simpson, Y. Wang, D. Rhodes, K. Fujisawa, L. Balicas, M. Dubey, V. H. Crespi, M. Terrones, A. R. Hight Walker, Nano Lett. 2017, 17, 5897.

[6] A. Yang, J. Gao, B. Li, J. Tan, Y. Xiang, T. Gupta, L. Li, S. Suresh, J. C. Idrobo, T. M. Lu, M. Rong, N. Koratkar, 2D Mater. 2016, 3, 045012.

[7] Q. Kuang, C. Lao, L. W. Zhong, Z. Xie and L. Zheng, J. Am. Chem. Soc. 2007, 129, 6070.

[8] J. L. Fu and F. Ayazi, in Proceedings of IEEE Sensors, 2010, pp. 2131.

[9] C. L. Cao, C. G. Hu, L. Fang, S. X. Wang, Y. S. Tian and C. Y. Pan, J. Nanomater. 2011, 5, 2011.

[10] Y. Yao, X. Chen, H. Guo and Z. Wu, Appl. Surf. Sci. 2011, 257, 7778.

[11] D. J. Late, Y. K. Huang, B. Liu, J. Acharya, S. N. Shirodkar, J. Luo, A. Yan, D. Charles, U. V. Waghmare, V. P. Dravid and C. N. R. Rao, ACS Nano, 2013, 7, 4879.

[12] W. Xuan, M. He, N. Meng, X. He, W. Wang, J. Chen, T. Shi, T. Hasan, Z. Xu, Y. Xu and J. K. Luo, Sci. Rep. 2014, 4, 1.

[13] D. Zhang, J. Tong and B. Xia, Sensors Actuators, B Chem. 2014, 197, 66.

[14] W. H. Lim, Y. K. Yap, W. Y. Chong and H. Ahmad, Sensors, 2014, 14, 24329.

[15] M. S. Pawar, P. K. Bankar, M. A. More and D. J. Late, RSC Adv. 2015, 5, 88796.

[16] D. J. Late, Microporous Mesoporous Mater. 2016, 225, 494.

[17] A. De Luca, S. Santra, R. Ghosh, S. Z. Ali, J. W. Gardner, P. K. Guha and F. Udrea, Nanoscale, 2016, 8, 4565.

[18] T. Islam and M. Z. Ur Rahman, IEEE Trans. Instrum. Meas. 2016, 65, 694.

[19] M. B. Erande, M. S. Pawar and D. J. Late, ACS Appl. Mater. Interfaces, 2016, 8, 11548.

[20] A. Yang, J. Gao, B. Li, J. Tan, Y. Xiang, T. Gupta, L. Li, S. Suresh, J. C. Idrobo, T. M. Lu, M. Rong and N. Koratkar, 2D Mater. 2016, 3, 045012.

[21] K. Shehzad, T. Shi et al., Adv. Mater. Technol. 2017, 2, 1600262.

[22] A. D. Smith, K. Elgammal, F. Niklaus, A. Delin, A. C. Fischer, S. Vaziri, F. Forsberg, M. Råsander, H. Hugosson, L. Bergqvist, S. Schröder, S. Kataria, M. Östling, M. C. Lemme, Nanoscale 2015, 7, 19099.

[23] J. Wu, Z. Wu, H. Xu, Q. Wu, C. Liu, B. R. Yang, X. Gui, X. Xie, K. Tao, Y. Shen, J. Miao, L. K. Norford, Mater. Horizons 2019, 6, 595.

[24] D. J. Late, A. Ghosh, B. Chakraborty, A. K. Sood, U. V. Waghmare, C. N. R. Rao, J. Exp. Nanosci. 2011, 6, 641.

[25] L. Khandare, S. S. Terdale, and D. J. Late, Adv. Device Mater. 2016, 2, 15.

Chapter 3

Light-Assisted and Gate-Tunable Oxygen Gas Sensors Based on Rhenium Disulfide Field-Effect Transistors

Chapter 3 reports about Light-Assisted and Gate-Tunable Oxygen Gas Sensors Based on Rhenium Disulfide Field-Effect Transistors. It is divided into several sections, namely introduction, experimental, results and discussions, conclusion, and supplementary data. The experimental section is divided into sub-section namely gas sensing measurement of ReS_2-FET based oxygen sensor. Meanwhile, the section of results and discussions section is divided into sub-sections of structural properties, electrical and sensing properties, and stability and durability properties of ReS_2-FET based on oxygen sensor. The section of supplementary data is divided into the influence of ReS_2 thickness and light intensity on oxygen sensing performance, and advantage of gate-bias and light illumination for device stability under humid environment. The details for each section are described as below.

3.1. Introduction

In the previous chapter, the utilization of gate biasing operation of sensitive ReS_2-FET humidity sensor has been discussed. The concept of gate biasing operation for improving the gas sensitivity has been described. To this extend, in this chapter, we extend our investigation toward light-assisted and gate-tunable oxygen gas sensors based on ReS_2-FETs. As mentioned in the chapter 1, oxygen gas sensors are essential for a wide range of applications related to, for example, medicine, automobiles, food, and the environment.[1–5] Many studies have reported about the improvement of gas sensitivity by light illumination and gate biasing. However, although the enhancement of the gas

sensitivity of TMDC-based FETs by light illumination and gate biasing has been reported, the mechanism and roles of their combined effects are not yet understood.[6–11]

In this chapter, we investigated ReS_2-FET based oxygen gas sensor devices under the aid of gate bias and light illumination conditions. The sensing performance, including response, sensitivity, stability, and durability, was studied in a systematic manner. We focused particularly on the light illumination and gate voltage dependence to clarify their roles in the sensing mechanism. As a result, a practical sensitivity of 0.01% ppm^{-1} was achieved for oxygen gas by combining light illumination and a positive gate voltage, which outperform over previous reports.[12,13] This chapter also contributes to an in-depth understanding of the roles of light illumination and gate biasing, leading to the development of a high-performance gas sensor based on TMDC FETs.

3.2. Experimental

3.2.1. Sensing measurement of ReS_2-FET based oxygen sensor

The homemade gas measurement setup was equipped with a mixing connector linked to mass flow controllers that made it possible to adjust the oxygen concentration by changing the O_2/N_2 gas mixing ratio (**Figure 3-1**a). A constant flow rate of 100 mL min^{-1} was used for dry air and oxygen gas sensing measurement. The gas chamber was flushed with nitrogen for a few hours to recover the device to the initial state after each measurement. The setup was also equipped with a relative humidity (RH) controller. The RH levels were monitored with a commercial humidity sensor. All the current–voltage (*I–V*) measurements were carried out at room temperature using a source-measurement unit (Keysight B2912A), which was connected to a data acquisition system using EasyEXPERT software. A Xenon lamp (Asahi spectra Co. Ltd., LAX 102) was used for

light irradiation. The sensor was illuminated with red light at a wavelength of 650 nm through the acrylic resin window of the gas sensor chamber. The light intensity was monitored with a power meter (Ophir Optics, PD300).

3.3. Results and discussion

3.3.1. Structural properties of ReS_2-FET based oxygen sensor

Figure 3-1a shows a homemade chamber setup (dimensions: 9.0 x 6.0 x 2.5 cm^3) that used for the ReS_2-FET based oxygen sensor measurements. **Figure 3-1**b shows a Raman spectrum of the ReS_2 nanosheet, which displays 18 first-order modes within 100-450 cm^{-1}. All the Raman peaks are of Ag symmetry.[14] This labeling Raman peaks scheme was adopted from the previous report.[15] The in-plane, out-of-plane, and quasi-out-of-plane modes near 150, 437, and 418 cm^{-1} are labeled as A_{1g}, A_{2g}, and A_{3g}, respectively. This result confirmed the high crystallinity and chemical purity of the ReS_2 nanosheet.[16] **Figure 3-1**c shows an atomic force microscopy (AFM) image and the height profile (green line in the AFM image) of the ReS_2 nanosheet. The height profile confirmed that the ReS_2 thickness was ca. 6 nm, corresponding to eight-layer-thick ReS_2. The eight-layer ReS_2 nanosheet was used for all the oxygen sensing measurements in this chapter study, because this thickness was found to be optimal (See **Figure S3-1**, section of supplementary data section in this chapter for the study of the thickness-dependent on oxygen sensing properties).

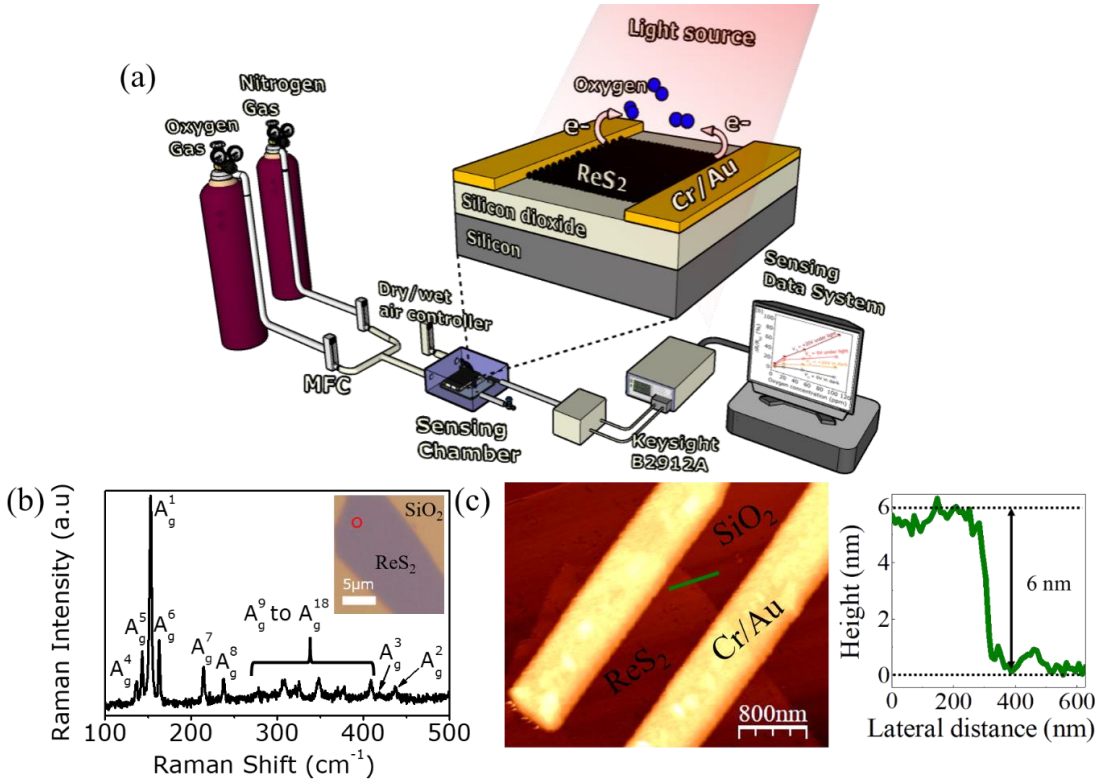

Figure 3-1. (a) Schematic diagram of the home-made gas sensing measurement setup and the ReS_2-FET based oxygen sensor. (b) Raman spectrum of the ReS_2 nanosheet obtained at the location indicated by the red circle seen in the inset optical image. (b) AFM image and height profile of the 8-layer ReS_2 nanosheet. (Reproduced from ref. [17], Copyright 2020, with the permission from Wiley-VCH GmbH Publisher).

3.3.2. Electrical and sensing properties of ReS_2-FET based oxygen sensor

Initially, the transfer curve was measured in a dark condition without oxygen exposure as a reference as shown in **Figure 3-2**a. A typical *n*-type operation was observed, i.e., electrons were majority carriers in the ReS_2-FET. Then, the influence of light illumination on oxygen sensing was examined. **Figure 3-2**b and **3-2**c show the output characteristics of the ReS_2-FET in dark conditions and under light illumination, respectively, while no gate voltage was applied. As seen in **Figure 3-2**b, the drain current gradually decreased as the oxygen concentration increased from 0 to 10,000 ppm. These results were caused by the nature of the oxygen molecule as an electron acceptor.[18] That

is, electrons were transferred from the ReS_2 channel surface to the physically adsorbed oxygen molecules to increase the device resistance.

This tendency was enhanced by light illumination as shown in **Figure 3-2**c; the variations in the drain current were larger than those obtained under dark conditions. For a clear comparison, the response under both dark conditions and light illumination are plotted as a function of oxygen concentration in **Figure 3-2**d, where the oxygen response was determined as the resistance ratio ($\frac{\Delta R}{R_{N_2}}$) based on the following equation:

$$\frac{\Delta R}{R_{N_2}} = \left[\frac{R_{O_2} - R_{N_2}}{R_{N_2}} \times 100\right]\% \qquad (3-1)$$

where R_{N_2} and R_{O_2} are the channel resistances in nitrogen gas (oxygen concentration = 0) and oxygen gas, respectively. The response under dark conditions (black line) showed a slightly monotonical increase from 4% to 19% with increasing oxygen concentration. Meanwhile, light illumination yielded a response of 60% at an oxygen concentration of 10,000 ppm, which is three times higher than that measured under dark conditions. This improvement was achieved by the photo-generated carriers.[19] That is, light illumination increased the electron population in the ReS_2-FET, and these electrons were available to interact with oxygen gas molecules. This result clearly demonstrates the advantage of light-assisted gas sensing. For these experiments, the light intensity was fixed at 8.4 mW/cm^2 because the maximum response was observed at this intensity (See **Figure S3-2**, section of supplementary data for the details).

To examine the effect of the gate voltage on the oxygen sensing performance, the output characteristics were measured under dark conditions with negative (V_G = –20 V)

and positive (V_G = +20 V) gate voltages as shown in **Figure 3-3**a and **3-3**b, respectively. As can be seen, the variations in the drain current with a negative gate voltage were marginal. Meanwhile, a clear modulation was observed in the drain current with a positive gate voltage. This tendency is further confirmed by the response-oxygen concentration curves shown in **Figure 3-3**c. Here, the curve without a gate voltage (V_G = 0, black line) is duplicated from **Figure 3-2**c for comparison. The response was increased by 38% by a positive gate voltage, while a negative gate voltage reduced it to 13% at a 10,000-ppm oxygen concentration. The results can also be explained in terms of the electron population at the ReS_2/SiO_2 interface. The negative gate voltage depleted the electrons at the ReS_2/SiO_2 interface. As a result, oxygen gas molecules, which are electron acceptors, receive fewer electrons from the ReS_2-FET. In the meantime, the electrons accumulated at the ReS_2/SiO_2 interface under a positive gate voltage to promote electron transfer with oxygen gas molecules, which contributed to the increment in oxygen gas response.

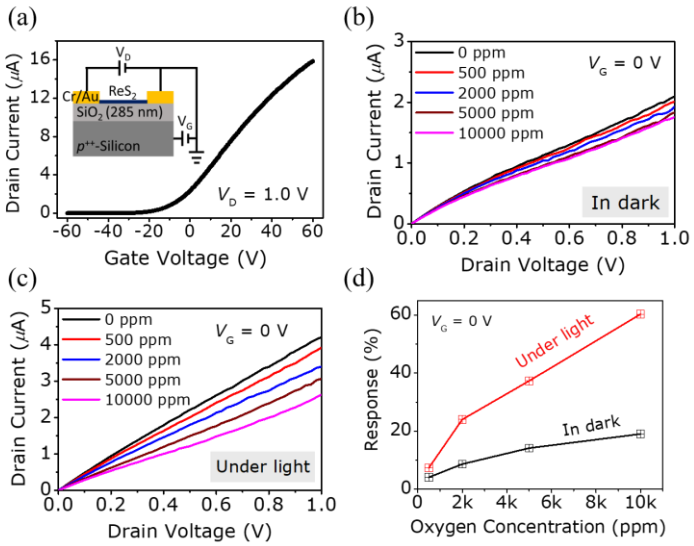

Figure 3-2. (a) Transfer curve of the 8-layer ReS_2-FET, and its output characteristics (b) in the dark and (c) with light illumination. The O_2 gas concentration ranged from 0 to 10,000 ppm. No gate voltage was applied. (d) Response as a function of O_2 gas concentration in the dark (black line) and with light illumination (red line).

(Reproduced from ref. [17], Copyright 2020, with the permission from Wiley-VCH GmbH Publisher).

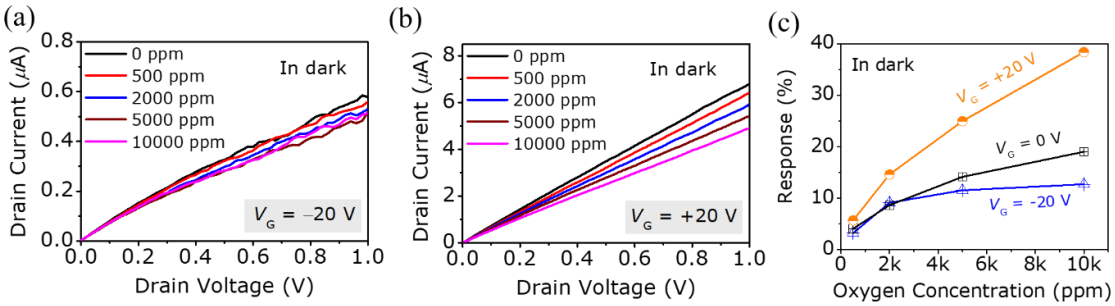

Figure 3-3. Output characteristics of the 8-layer ReS_2-FET under (a) V_G = –20 V, (b) V_G = +20 V and O_2 gas exposure at concentrations of 0 to 10,000 ppm measured in dark conditions. (c) Response as a function of O_2 gas concentration curves of the sensor with and without applying a gate voltage in dark conditions. (Reproduced from ref. [17], Copyright 2020, with the permission from Wiley-VCH GmbH Publisher).

Next, the combined effect of a positive gate voltage and light illumination on sensing performance was examined. **Figure 3-4**a shows the output characteristics of the ReS_2-FET measured with a combination of light illumination and a positive gate voltage (V_G = +20 V). A distinct decrease in the drain currents with increasing oxygen concentration was observed. **Figure 3-4**b summarizes response as a function of oxygen concentration. The ReS_2-FET operated under light illumination and a positive gate voltage exhibited improved oxygen gas response, which exceeded 100% at an oxygen concentration of 10,000 ppm. Namely, we achieved a sensitivity of 0.01% ppm^{-1}. This is higher than the value obtained in the dark with (0.003% ppm^{-1}) and without (0.002% ppm^{-1}) a gate voltage, and solely with light illumination (0.005% ppm^{-1}) (See **Figure S3-3**, section of supplementary data for the details).

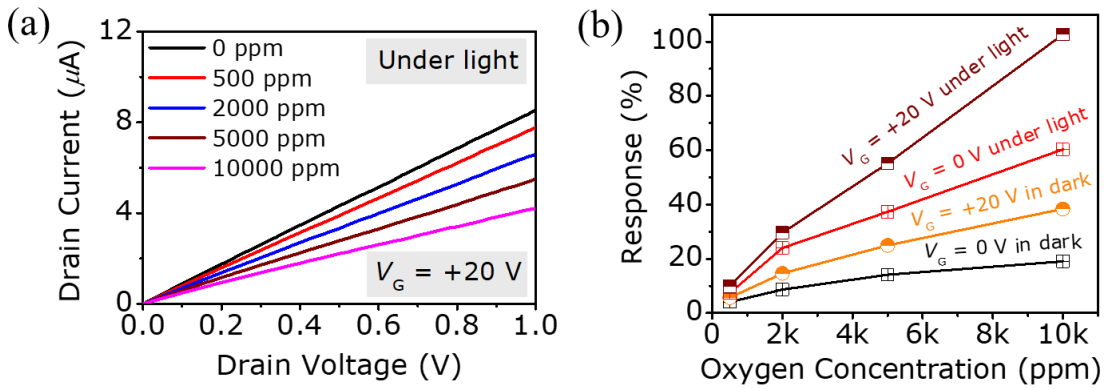

Figure 3-4. (a) Output characteristic of the 8-layer ReS_2-FET where V_G = +20 V and in an O_2 gas atmosphere at various concentrations ranging from 0 to 10,000 ppm measured under light illumination. (b) Response as a function of O_2 gas concentration when operated under various conditions: with/without gate voltage and with/without light illumination.

(Reproduced from ref. [17], Copyright 2020, with the permission from Wiley-VCH GmbH Publisher).

As mentioned above, the gas response is strongly related to the electron population in the ReS_2-FET. These phenomena can be further understood from the band diagrams shown in **Figure 3-5**. These band diagrams illustrate the interaction of the electrons in the conduction band of ReS_2 with oxygen gas on the ReS_2 surface. Under dark conditions without gate biasing (**Figure 3-5**a), the response is predominantly influenced by the doping effect of the gas molecules.[20] Meanwhile, the positive gate biasing leads to electron accumulation in ReS_2, which decreases R_{N_2} (**Figure 3-5**b). Then, the ReS_2 surface attracts the oxygen molecules, resulting in an increase in ΔR. Thus, the response ($\frac{\Delta R}{R_{N_2}}$) is enhanced. On the other hand, the light illumination also generates electrons by photo excitation, leading to the enhancement of $\frac{\Delta R}{R_{N_2}}$ (**Figure 3-5**c). The response is further improved by the combination of positive gate biasing and light illumination, which cause both the capacitively- and photo-induced electrons to accumulate (**Figure 3-5**d).

Consequently, a huge $\frac{\Delta R}{R_{N_2}}$ enhancement is accomplished. The oxygen sensing performance in this chapter study appears to be particularly noteworthy among reported sensors, which are summarized in **Table 3-1**.

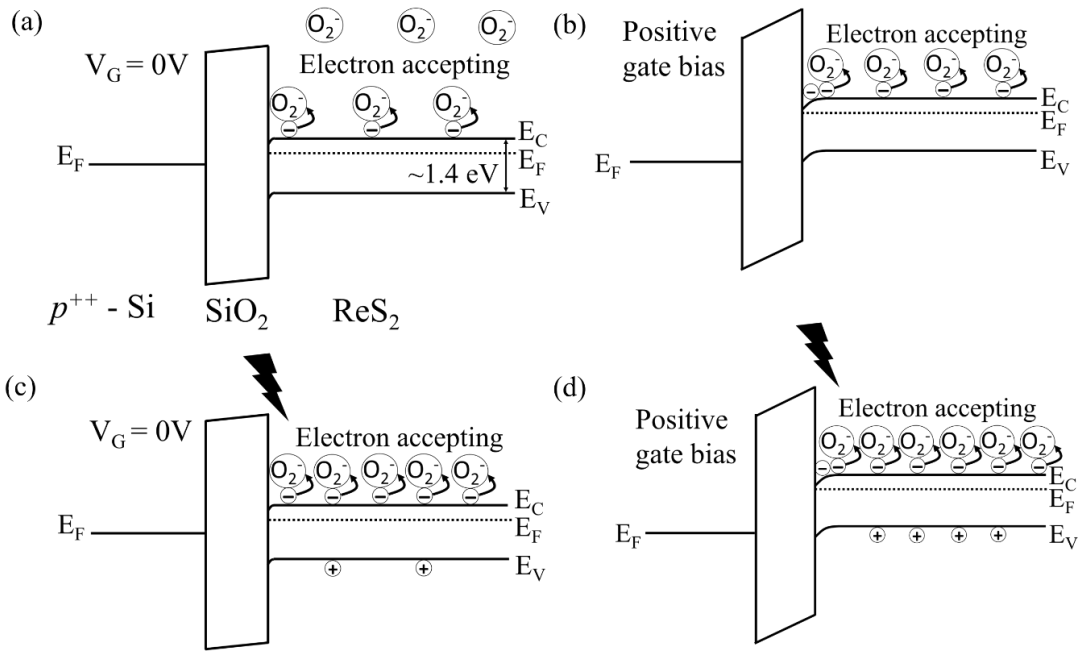

Figure 3-5. Band diagrams of the ReS_2-FET, illustrating the interaction of electrons in the ReS_2 with oxygen gas (a) under dark conditions without a gate bias, (b) under dark conditions with a positive gate bias, (c) under light illumination without a gate bias, and (d) under light illumination with a positive gate bias.

(Reproduced from ref. [17], Copyright 2020, with the permission from Wiley-VCH GmbH Publisher).

Table 3-1. Oxygen gas sensing properties of different oxygen gas sensors in the previous studies.

Sensing material	**Device type**	**Oxygen concentration**	**Response**	**Sensitivity**	**Operating temperature**	**Ref.**
$SrTiO_3$	Chemiresistor	20%	6.35 (R_{O2}/R_{N2})	---	40°C	[21] 2004
Pt-In_2O_3	Chemiresistor	20%	95% $(\Delta R/R_{N2})$	---	RT	[22] 2005
Pt-In_2O_3	Chemiresistor	20%	63.3% $(\Delta R/R_{N2})$	---	200°C	[23] 2007

Graphene/TiO_2	Chemiresistor	134 ppm	7% ($\Delta R/R_{N2}$)	---	RT	[18] 2013
ZnO	Chemiresistor	97%	419% ($\Delta R/R_{N2}$)	1.83%/%O_2	50°C / UV assisted	[3] 2014
MWCNTs/PVAc/TiO_2	Chemiresistor	5%	30 (R_{O2}/R_{N2})	---	400°C	[24] 2014
MoS_2	FET	9.9x10^{-5} millibars	29.2% ($\Delta I/I_{N2}$)	26.7x10^4% /mBar	RT / +40V gate-assisted	[12] 2015
MoS_2	Chemiresistor	100%	63.73% ($\Delta R/R_{N2}$)	0.545% /%O_2	300°C	[25] 2016
TiO_2	Chemiresistor	1%	1.15 (R_{O2}/R_{N2})	---	RT	[26] 2016
ReS_2	Chemiresistor	21%	-0.06 ($\Delta G/G_{inert}$)	---	RT	[27] 2019
TiS_2	Chemiresistor	1%	34.8% ($\Delta R/R_{N2}$)	1.75% /1.0%	RT	[13] 2020
ReS_2	FET	10,000 ppm	102.68% ($\Delta R/R_{N2}$)	0.01%/ppm	RT / light-assisted and gate-bias assisted	[17] 2020

(Reproduced from ref. [17], Copyright 2020, with the permission from Wiley-VCH GmbH Publisher).

Table 3-1 summarizes the oxygen sensing properties of different oxygen gas sensors described in previous reports. Our oxygen gas sensor, which operated under a combination of light illumination and a +20 V gate voltage, is noteworthy in terms of response and sensitivity as compared with the earlier reports.

3.3.3. Stability and durability properties of ReS_2-FET based oxygen sensor

The stability and durability of the ReS_2-FET based oxygen sensor properties are also vital for practical applications. To examine these factors, measurements were repeated in light illumination and positive gate voltage operations. The device was exposed to oxygen gas every week for 35 days in dry or humid conditions. As shown in

Figure 3-6a and **3-6**b, the response at an oxygen concentration of 10,000 ppm was retained after 35 days of measurement and it was largely unchanged even when measured in humid conditions. That is, our sensor showed long-term stability, and stable operation even under humid conditions. We suggest that this high stability is brought about by the advantages of gate biasing and light illumination in suppressing the electron transfer from the water molecules to the ReS_2 surface (See **Figure S3-4**, section of supplementary data for the details). The results imply that our sensor could be employed in real-time applications.

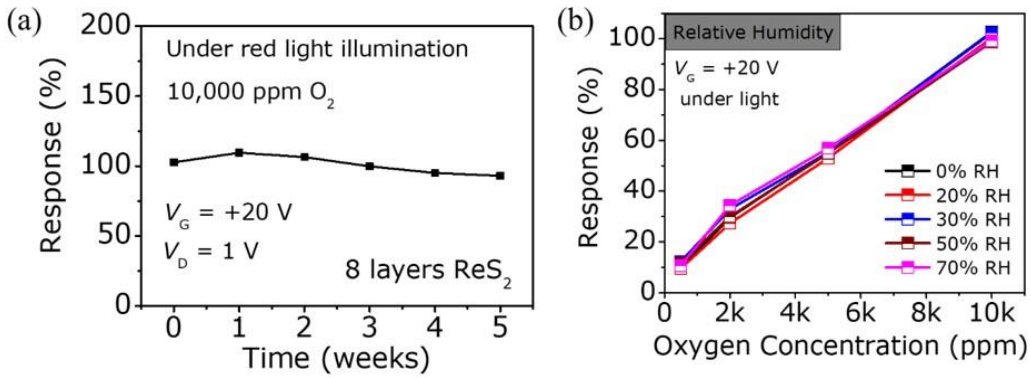

Figure 3-6. (a) Long-term stability test at 10,000 ppm O_2 gas concentration. (b) Influence of relative humidity on device response. The relative humidity was varied from 0% to 70% by controlling the mixture ratio of dry and wet air.

(Reproduced from ref. [17], Copyright 2020, with the permission from Wiley-VCH GmbH Publisher).

3.4. Conclusion

In conclusion, in this chapter, we have developed high-performance ReS_2-FET based oxygen sensors by combining light illumination and a gate biasing operation. The underlying mechanism was explained by the electron transfer from ReS_2 into oxygen molecules to stimulate changes in the transistor properties. Light illumination and gate biasing improved the oxygen sensing properties by increasing the photogenerated carrier and doping level of the ReS_2-FET. In consequence, a practical sensitivity of 0.01% ppm^{-}

[1] was achieved, which outperform results from the previous reports. Furthermore, long-term stability and stable operation even under humid conditions enabled the sensor device to be used in real-time applications. These results imply that a light-assisted and gate-bias-tunable oxygen sensor based on a ReS_2-FET has the potential for allowing further sensor development toward versatile tunable oxygen sensors. Future studies are yet to be considered for further understanding on gas sensing properties of ReS_2-FET. This including the angle-dependent study of ReS_2 anisotropic crystal lattice structure on gas sensing performance.

3.5. Supplementary data

3.5.1. Influence of ReS_2 thickness on oxygen sensing response

To clarify the role of ReS_2 thickness, 6-, 8- and 11-layer-thick ReS_2-FETs were prepared. The response of each sensor was examined under oxygen concentrations varying from 0 to 10,000 ppm as shown in **Figure S3-1**. All the gas sensing measurements were conducted out under light illumination and without a gate voltage. As the thickness was increased to 11 layers, the oxygen response of the device provided comparable data to that of an 8-layer ReS_2-FET, which suggested that 8-layer-thick ReS_2 is sufficient for use in a high-performance oxygen sensor.

This could be due to any of many factors such as the trade-off dependence between the surface-to-volume ratio[28] and the optical absorbance[29] on the light-assisted gas sensing properties. A high surface-to-volume ratio favors more gas adsorption on the channel surface and accelerates the charge accumulation to interact with gas molecules.[30] Meanwhile, the optical phenomena of few-layer ReS_2 (8 layers) is sufficient to obtain reasonable optical absorption,[16] which we assume to provide an

optimal optoelectrical response to the sensors compared with a monolayer in order to efficiently collect photogenerated carriers at the top electrodes.

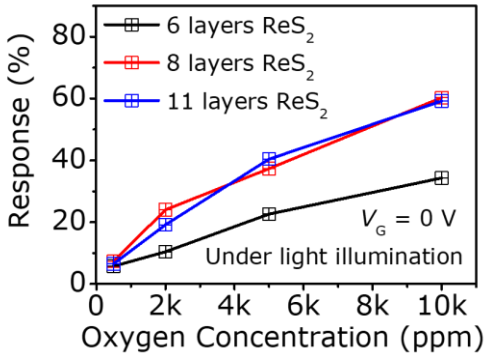

Figure S3-1. Response as a function of oxygen gas concentration (electron accepting behavior) for 6-, 8-, and 11-layer ReS_2-FETs.

(Reproduced from ref. [17], Copyright 2020, with the permission from Wiley-VCH GmbH Publisher).

3.5.2. Influence of light intensity on oxygen sensing response

To clarify the influence of light intensity on the oxygen sensing response, an 8-layer ReS_2-FET was exposed to oxygen gas concentrations ranging from 0 to 10,000 ppm under illumination with four different light intensities: 1.6, 5.6, 8.4 and 12.0 mW/cm^2, as shown in **Figure S3-2**. It is apparent that the optimal response toward oxygen gas was achieved at 8.4 mW/cm^2 by comparison with that at 1.6, 5.6, and 12 mW/cm^2.

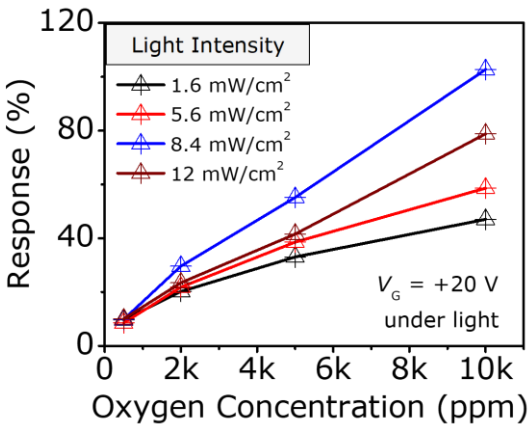

Figure S3-2. Influence of light intensity variation on 8-layer ReS_2-FET sensor device response.

(Reproduced from ref. [17], Copyright 2020, with the permission from Wiley-VCH GmbH Publisher).

The oxygen gas sensitivity (S_{O2}) was obtained from the slope of the line between the response and oxygen concentration by using the following equation:

$$S_{O2} = \left[\frac{\partial\,(\Delta R/R_{N2})}{\partial\,C_{O2}}\right] \qquad (3-2)$$

where C_{O2} represents oxygen concentration.

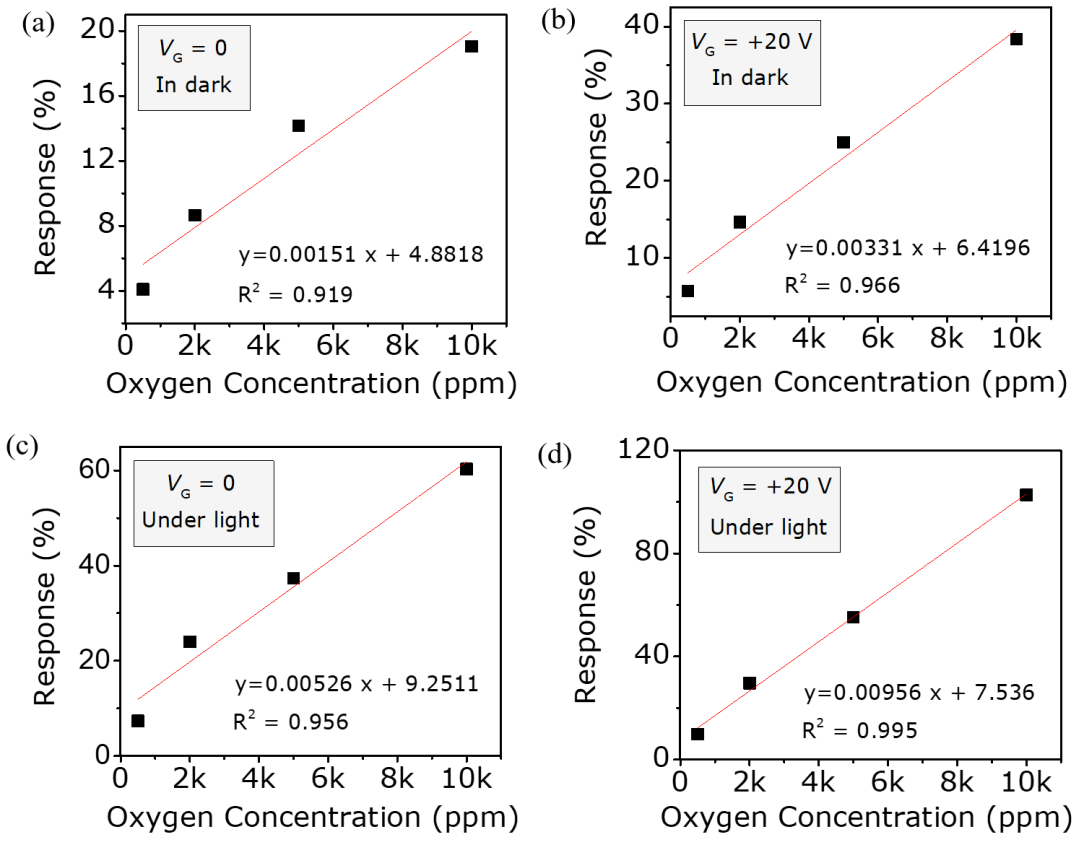

Figure S3-3. Linear fit curves of the response value as a function of oxygen concentration under different operating conditions: (a) in the dark without a gate bias, (b) in the dark with a +20 V gate bias, (c) under light without a gate bias, and (d) under light with a +20 V gate bias. The sensor response exhibited linear behaviors. These behaviors show that the sensor device can be sensitively and reliably operated over a wide concentration range.

(Reproduced from ref. [17], Copyright 2020, with the permission from Wiley-VCH GmbH Publisher).

3.5.3. Advantage of gate biasing and light illumination for device stability under humid environment

As reported in the previous reports, ReS_2 is sensitive to water/moisture, in which water molecules behave as an electron donor.[27,31] Thus, the drain current of the ReS_2-FET increased with increasing relative humidity (RH). However, these sensing measurements were conducted in dark condition with no gate biasing.

To clarify the advantage of gate biasing and light illumination for device stability under humid environment, RH sensing measurements of ReS_2-FETs under various sensing measurement were carried out as shown in **Figure S3-4**.

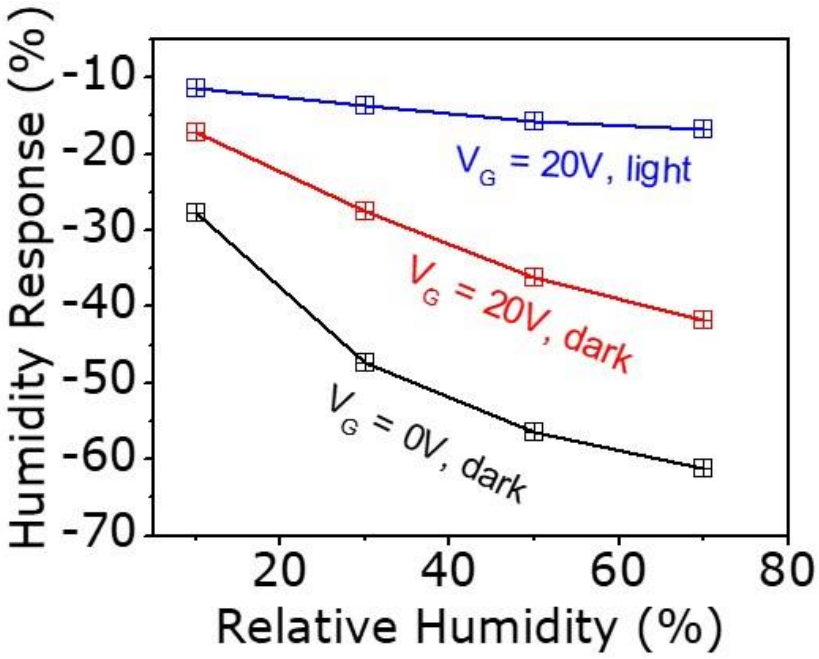

Figure S3-4. Humidity response curve as a function of relative humidity under various sensing measurements: in dark and under light illumination with/without gate voltage.

(Reproduced from ref. [17], Copyright 2020, with the permission from Wiley-VCH GmbH Publisher).

RH response was calculated with the following equation:

$$Humidity\ Response = \left[\frac{R_{H_2O} - R_{dry}}{R_{dry}} \times 100\right]\% \qquad (3-3)$$

Where R_{H_2O} and R_{dry} are the channel resistance in humid vapor and dry air, respectively. RH response in dark with no gate biasing decreased monotonically with increasing RH (black line), which follow the trend in the previous report.[27,31] This tendency was increased by applying a positive gate voltage (red line), which reduced the channel resistance. Then, by applying light illumination with positive gate voltage (blue line), the device exhibited insensitive toward RH humidity changes. The reason is suggested to be related to the coverage of the water molecules in which electron transfer from water molecules was suppressed.

To emphasize, a positive gate voltage and light illumination prevented the variation in RH response. When a positive gate voltage was applied, the electrons accumulated at the ReS_2-SiO_2 interface, which led to reduction of R_{dry}. Therefore, humidity sensitive was decreased. The humidity sensitive was further decreased by the combination of positive gate biasing and light illumination, which cause both the capacitive-induced and photo-induced electrons to accumulate. These conditions suppressed the electron transfer from the water molecules, thus make the device insensitive to RH changes even under humid conditions.

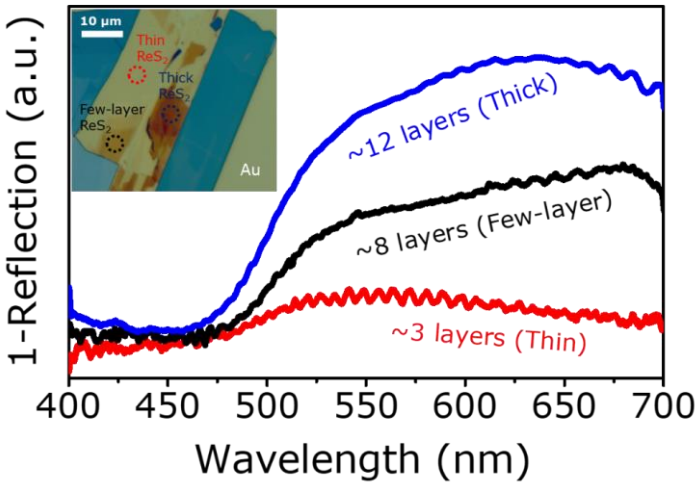

Figure S3-5. Absorption spectra (1-Reflection) of ReS_2 nanosheets. Inset is an optical image showing thin-layer, a few-layer and thick-layer ReS_2 on top of a Au film coated substrate. Light illumination of 650 nm wavelength was utilized for oxygen sensing measurement of 8-layer ReS_2-FET, which observed to provide reasonable absorption.

(Reproduced from ref. [17], Copyright 2020, with the permission from Wiley-VCH GmbH Publisher).

(The content in this chapter is reproduced from [17], Copyright 2020, with permission from Wiley-VCH GmbH Publisher*)*

References

[1] Y. Liu, J. Parisi, X. Sun, Y. Lei, *J. Mater. Chem. A* **2014**, *2*, 9919.

[2] A. W. Hempel, D. B. Papkovsky, J. P. Kerry, *foods* **2013**, *2*, 507.

[3] C. S. Chou, Y. C. Wu, C. H. Lin, *RSC Adv.* **2014**, *4*, 52903.

[4] C. A. Kelly, E. Santovito, M. Cruz-Romero, J. P. Kerry, D. P. Papkovsky, *Sensors Actuators, B Chem.* **2020**, *304*, 127338.

[5] M. Bartic, *Phys. Status Solidi Appl. Mater. Sci.* **2016**, *213*, 457.

[6] W. J. Yan, D. Y. Chen, H. R. Fuh, Y. L. Li, D. Zhang, H. Liu, G. Wu, L. Zhang, X. Ren, J. Cho, M. Choi, B. S. Chun, C. Coileáin, H. J. Xu, Z. Wang, Z. Jiang, C. R. Chang, H. C. Wu, *RSC Adv.* **2019**, *9*, 626.

[7] M. Kumar, A. V. Agrawal, R. Kumar, S. Venkatesan, A. Zakhidov, G. Yang, J. Bao, M. Kumar, *ACS Sensors* **2018**, *3*, 998.

[8] S. Yang, J. Kang, Q. Yue, J. M. D. Coey, C. Jiang, *Adv. Mater. Interfaces* **2016**.

[9] Z. Feng, Y. Xie, J. Chen, Y. Yu, S. Zheng, R. Zhang, Q. Li, X. Chen, C. Sun, H. Zhang, W. Pang, J. Liu, D. Zhang, *2D Mater.* **2017**, *4*, 025018.

[10] X. Yan, Y. Wu, R. Li, C. Shi, R. Moro, *ACS Omega* **2019**, *4*, 14179−14187.

[11] T. Pham, G. Li, E. Bekyarova, M. E. Itkis, A. Mulchandani, *ACS Nano* **2019**, *13*, 3196.

[12] Y. Tong, Z. Lin, J. T. L. Thong, D. S. H. Chan, C. Zhu, *Appl. Phys. Lett.* **2015**, *107*, 123105.

[13] N. Sakhuja, R. K. Jha, R. Chaurasiya, A. Dixit, N. Bhat, *ACS Appl. Nano Mater.* **2020**, *3*, 3382.

[14] N. R. Pradhan, A. McCreary, D. Rhodes, Z. Lu, S. Feng, E. Manousakis, D. Smirnov, R. Namburu, M. Dubey, A. R. Hight Walker, H. Terrones, M. Terrones,

V. Dobrosavljevic, L. Balicas, *Nano Lett.* **2015**, *15*, 8377.

[15] A. McCreary, J. R. Simpson, Y. Wang, D. Rhodes, K. Fujisawa, L. Balicas, M. Dubey, V. H. Crespi, M. Terrones, A. R. Hight Walker, *Nano Lett.* **2017**, *17*, 5897.

[16] B. Mukherjee, A. Zulkefli, R. Hayakawa, Y. Wakayama, S. Nakaharai, *ACS Photonics* **2019**, *6*, 2277.

[17] M. A. Zulkefli, B. Mukherjee, R. Hayakawa, T. Iwasaki, S. Nakaharai, Y. Wakayama, *Phys. Status Solidi - Rapid Res. Lett.* **2020**, 2000330.

[18] J. Zhang, C. Zhao, P. A. Hu, Y. Q. Fu, Z. Wang, W. Cao, B. Yang, F. Placido, *RSC Adv.* **2013**, *3*, 22185.

[19] N. Huo, S. Yang, Z. Wei, S.-S. Li, J.-B. Xia, J. Li, *Sci. Rep.* **2014**, *4*, 5209.

[20] Y. Cai, Q. Ke, G. Zhang, Y. W. Zhang, *J. Phys. Chem. C* **2015**, *119*, 3102.

[21] Y. Hu, H. Lee, S. Kim, M. Yun, *Sensors Actuators B. Chem.* **2013**, *181*, 424.

[22] G. Neri, A. Bonavita, G. Micali, G. Rizzo, S. Galvagno, M. Niederberger, N. Pinna, *Chem. Commun.* **2005**, *48*, 6032.

[23] G. Neri, A. Bonavita, G. Micali, G. Rizzo, N. Pinna, M. Niederberger, *Sensors Actuators, B Chem.* **2007**, *127*, 455.

[24] P. Frontera, S. Trocino, A. Donato, P. L. Antonucci, M. Lo Faro, G. Squadrito, G. Neri, *Electron. Mater. Lett.* **2014**, *10*, 305.

[25] Y. H. Kim, K. Y. Kim, Y. R. Choi, Y. S. Shim, J. M. Jeon, J. H. Lee, S. Y. Kim, S. Han, H. W. Jang, *J. Mater. Chem. A* **2016**, *4*, 6070.

[26] H. Wang, Y. Yao, G. Wu, Q. Sun, M. Wang, X. Chen, J. Wang, In *IEEE 3M-NANO 2016 - 6th IEEE International Conference on Manipulation, Manufacturing and Measurement on the Nanoscale*, IEEE, **2017**, pp. 199–202.

[27] B. Martín-garcía, D. Spirito, S. Bellani, M. Prato, V. Romano, A. Polovitsyn, R.

Brescia, R. Oropesa-nuñez, L. Najafi, A. Ansaldo, G. D. Angelo, V. Pellegrini, R. Krahne, I. Moreels, F. Bonaccorso, *Small* **2019**, *15*, 1904670.

[28] S. Yang, J. Kang, Q. Yue, J. M. D. Coey, C. Jiang, *Adv. Mater. Interfaces* **2016**, *3*, 1500707.

[29] M. Donarelli, L. Ottaviano, *Sensors* **2018**, *18*, 3638.

[30] K. Y. Ko, J. G. Song, Y. Kim, T. Choi, S. Shin, C. W. Lee, K. Lee, J. Koo, H. Lee, J. Kim, T. Lee, J. Park, H. Kim, *ACS Nano* **2016**, *10*, 9287.

[31] A. Yang, J. Gao, B. Li, J. Tan, Y. Xiang, T. Gupta, L. Li, S. Suresh, J. C. Idrobo, T. M. Lu, M. Rong, N. Koratkar, *2D Mater.* **2016**, *3*, 045012.

Chapter 4

Enhanced Selectivity in Volatile Organic Compound (VOCs) Gas Sensors based on ReS_2-FETs under Light-Assisted and Gate-Bias Tunable Operation

Chapter 4 reports about Enhanced Selectivity in Volatile Organic Compound (VOCs) Gas Sensors based on ReS_2-FETs under Light-Assisted and Gate-Bias Tunable Operation. It is divided into several sections, namely introduction, experimental, results and discussions, conclusion, and supplementary data. The experimental section is divided into sub-section namely gas sensing measurement setup, measurement of electrical and photoelectrical properties, gas sensing test, and DFT calculation. Meanwhile, the section of results and discussions section is divided into sub-sections of structural properties, electrical and sensing properties, and stability and durability properties of ReS_2-FET based on VOCs gas sensor. The section of supplementary data is divided into the influence of ReS_2 thickness and light intensity on VOCs gas sensing performance. The details for each section are described as below.

4.1. Introduction

A volatile organic compound (VOC) is a chemical reagent commonly used in industrial processing, research laboratory, hygienic products, etc. Long-term exposure to such chemical reagents can cause severe health issues such kidney failure and nerve damage. So far, the detection of these chemical reagents is widely used in medical field, pharmacology, and cosmetics production for safety purpose. Nevertheless, conventional gas sensing-methods, such as gas chromatography-mass spectroscopy has drawbacks

including device complexity, large size, and selectivity issue. Therefore, developing an approach for selective gas detection with a simple device structure is required.

In this chapter, the advantages of ReS_2's effective response to light illumination to improve the selectivity of a ReS_2-FET device's gas-sensing efficiency are highlighted. We found that the light illumination modulates the drain current response in a ReS_2-FET to adsorbed molecules, and the sensing activity differs depending on the gas species used, such as acetone, ethanol and methanol. Furthermore, wavelength and carrier density rely on certain variations in light-modulated sensing behaviors for each chemical. The device will distinguish the gas concentration in a mixture of VOCs using the differences induced by light illumination, enhancing the selectivity of the sensor device. By focusing on the specific device concept of light illumination, our results shed new light on the sensing technologies for realizing a large-scale sensor network in the Internet-of-Things era.

4.2. Experimental

4.2.1. Gas sensing measurement setup

A triple-line VOC delivery setup was used (**Figure 4-1**). A pure carrier nitrogen gas was bubbled into the VOC liquid to introduce the VOC gas into the gas chamber. To control the relative humidity level, the first and second lines control the dry air and wet airlines, respectively. The third line is used as the VOCs output terminal. To ensure that no apparent vapor drifts during the sensing measurement, the VOC glass bubbler was kept in good contact with a temperature-controlled oil bath and maintained at room temperature. Meanwhile, the device was wire-bonded on a chip carrier and then mounted on the chip carrier holder. After each measurement, the gas chamber was flushed with nitrogen gas for a few minutes to recover the sensor.

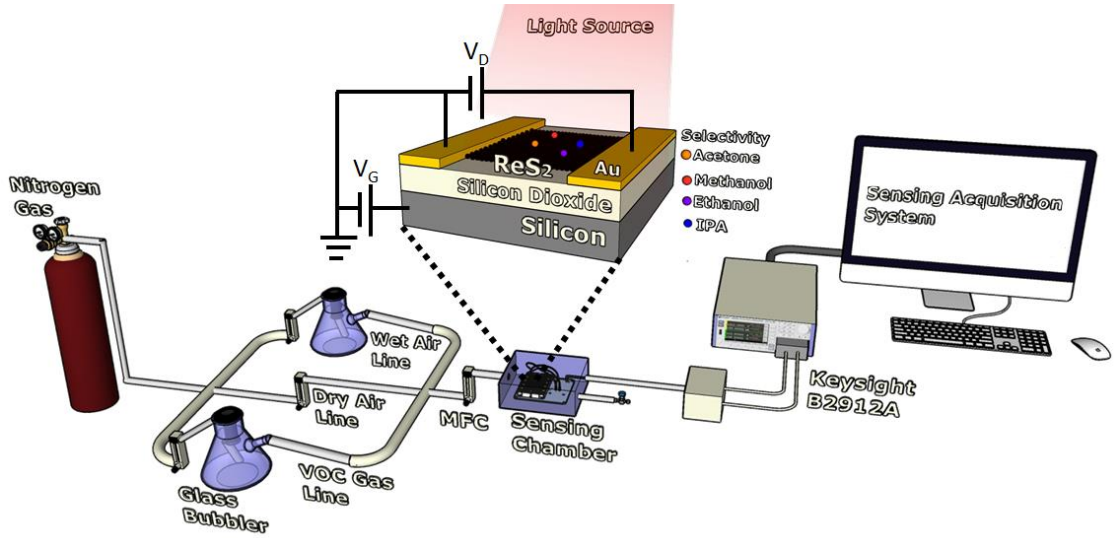

Figure 4-1. Schematic illustration demonstrating the gas sensing measurement setup and the VOCs gas sensor based ReS_2-FET.

(Reproduced from ref. [1], ACS Applied Materials &Interfaces, Submitted: June 2021).

4.2.2. Electrical, photoelectrical properties measurement and gas sensing test

A source-measurement unit was used to measure the output and transfer curves in the dark and under light illumination (Keysight B2912A). A Xenon light source (Asahi spectra Co. Ltd., LAX 102) was used for light illumination. All the VOC gas-sensing measurements were performed using a homemade gas-sensing setup. All tests were performed in the same environment at room temperature and a controlled relative humidity of ~50%.

4.2.3. DFT calculation

A 5×5×1 ReS_2 supercell model was constructed with a vacuum thickness set to 23 Å. First principles calculation based on density functional theory (DFT) was performed using Vienna ab initio simulation package.[2,3] The projector augmented wave method [3,4]

was used to describe electron-ion interactions. For exchange and correlation energy calculations, generalized gradient approximation (GGA) formulated by Perdew, Burke, and Ernzerhof was employed.[5] Van der Waals corrections were considered within Tkatchenko-Scheffler method with iterative Hirshfeld partitioning.[6] Full ionic relaxation was performed for the structure with 2×2×1 k-points as the mesh grid of the Brillouin zone. The cutoff energy was 500eV, while the convergence criteria on the total energy and interatomic forces ware 10^{-5} eV and 10^{-4} eV/Å^{-1}, respectively. The optimized structures were drawn using VESTA software.[7]

4.3. Results and discussion

4.3.1. Structural properties of ReS_2-FET based VOCs gas sensor

Figures 4-2a and **4-2**b show the schematic diagram and a reflection-mode optical image of ReS_2-FET, respectively. **Figure 4-2**c shows atomic force microscopy (AFM) image of the ReS_2 nanoflake and its height profile (along the green line in the AFM image). The ReS_2 layer thickness of approximately 6 nm was confirmed (ca. 8-layer-thick ReS_2). The thickness was fixed at 6 nm because the optimal response was observed by using this thickness (see Supplementary Data section for the thickness-dependent study on the gas sensing performance). **Figure 4-2**d shows the Raman spectrum of the ReS_2 nanoflake. Here, 18 first-order of A_g symmetry modes were demonstrated within 100–450 cm^{-1}.[8] The in-plane, out-of-plane and quasi-out-of-plane vibrational modes at 152 cm^{-1}, 438 cm^{-1} and 417 cm^{-1} are labelled as A_g^1, A_g^2 and A_g^3, respectively, which confirmed the high chemical purity and crystallinity of the ReS_2 nanoflake.[8,9]

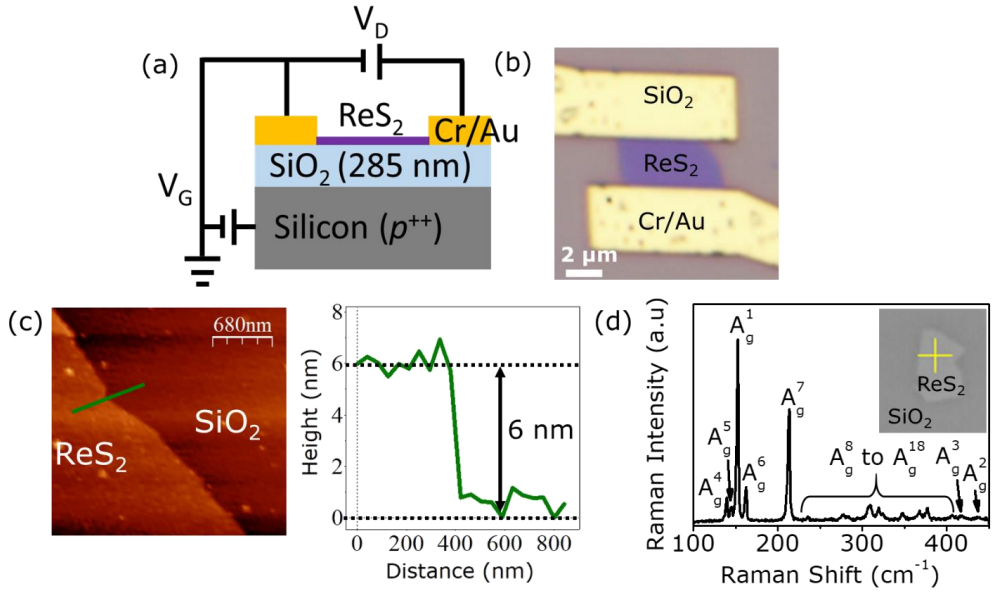

Figure 4-2. (a) Schematic diagram and (b) optical image of ReS_2-FET. (c) Atomic force microscopy image and its height profile of the ReS_2 nanosheet 6 nm thick. (d) Raman spectra of ReS_2 crystals taken from location as indicated by yellow plus symbol in the inside image.

(Reproduced from ref. [1], ACS Applied Materials &Interfaces, Submitted: June 2021).

4.3.2. Electrical and sensing properties of ReS_2-FET based VOCs gas sensor

Initially, a series of electrical measurements were performed to examine the FET and photoelectrical performances of ReS_2 devices. **Figures 4-3**a and **4-3**b present the initial output and transfer curves, respectively, measured in a dark condition. A typical ohmic contact between the ReS_2 channel and metal electrode and *n*-type transistor operation was observed. **Figure 4-3**c shows the photocurrent (I_{ph}) vs. gate bias of ReS_2-FET under light illumination with wavelengths; λ = 340 nm, 400 nm and 650 nm at a fixed light intensity of 8.4 mW/cm^2. The device displays gate bias-dependent light sensitivity with maximum light sensitivity at λ = 650 nm due to photon energy matching the bandgap of a few-layers ReS_2. Furthermore, photocurrent has no wavelength dependency at V_g = –40 V. However, it does at +40 V. This is because the *n*-ReS_2 channel is completely depleted at sufficiently high turn OFF voltage (–40 V gate bias), and no

majority carrier electrons from photogeneration are produced under different wavelength excitation, resulting in no wavelength dependence. The increase in photocurrent at zero gate bias (turn ON condition) can be explained by increasing the ReS_2 absorption coefficient from 340 nm to 650 nm wavelength. Additionally, if the turn ON voltage is high enough (+40 V gate bias), all of the interface trap states will be filled, causing the density of high-intensity light-induced carriers to saturate, resulting in photocurrent saturation at 650 nm.[10] On the other side, the filled interface trap states are de-trapped and recombine with photogenerated holes in the UVA region (320–400 nm), effectively reducing the saturation current.[11]

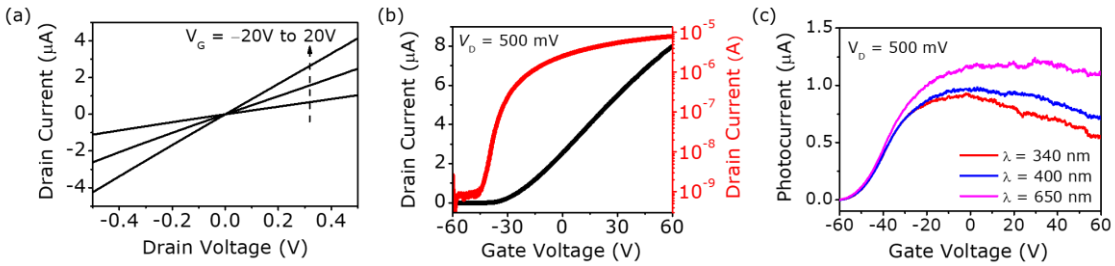

Figure 4-3. Output characteristics of 8 layers ReS_2-FET. (b) Transfer characteristics of 8 layers ReS_2-FET in linear (black line) and logarithmic (red line) scales. The measurements were conducted under dark conditions. (c) Photoelectrical characteristics of 8 layers ReS_2-FET under different wavelengths (λ = 340 nm, 400 nm, and 650 nm). All measurements were conducted at room temperature and controlled relative humidity level (50%RH).

(Reproduced from ref. [1], ACS Applied Materials &Interfaces, Submitted: June 2021).

The gas sensing of VOCs was examined using a gas-sensing device in a dark and zero gate-bias condition using a gas sensing system as illustrated in **Figure 4-1**. A detailed description of the gas-sensing measurement setup can be found in the Experimental Section. The output characteristics of the ReS_2-FET for acetone, methanol, ethanol and IPA vapors are shown in **Figures 4-4**a, **4-4**b, **4-4**c and **4-4**d, respectively. These current-

voltage characteristics were measured in 0–100 ppm. The drain current gradually decreases as the acetone and methanol concentration increased (**Figure 4-4**a and **4-4**b), while **Figure 4-4**c observed the opposite, i.e. the drain current gradually increases as the ethanol concentration increases. These results were caused by the nature of the acetone and methanol as electron acceptors. Meanwhile, when exposed to ethanol, ethanol molecule with low electron affinity acts as an electron donor, transferring electrons to the *n*-type ReS_2 conduction band and lowering device resistances.[12,13] Furthermore, **Figure 4-4**d shows a device that is insensitive to isopropanol (IPA). The response and sensitivity (S_{gas}) of these different gases' exposure are plotted as a gas concentration function in **Figures 4-4**e and **4-4**f, respectively, for a better comparison. The response was obtained as the relative resistance change calculated based on the following equation:

$$\frac{\Delta R}{R_O} = \left[\frac{R_{gas} - R_O}{R_O} \times 100\right]\% \qquad (4-1)$$

where R_{gas} and R_O refer to the channel resistance with and without VOC gas exposure, respectively. Meanwhile, S_{gas} was obtained from the slope of the line between the gas response and concentration by using the following equation:

$$S_{gas} = \left[\frac{\partial\,(\Delta R/R_O)}{\partial\,C_{gas}}\right] \qquad (4-2)$$

where C_{gas} refer to VOCs gas concentration.

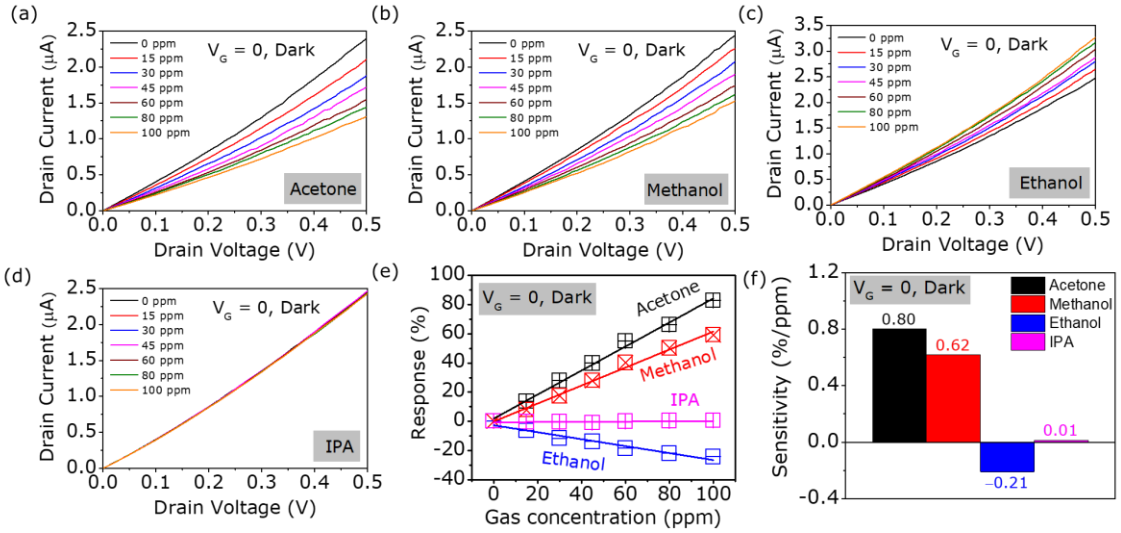

Figure 4-4. Two-probe drain current-voltage characteristics of 8 layers ReS_2-FET under different VOC gases: (a) acetone, (b) methanol, (c) ethanol and (d) IPA. The gas concentration ranges from 0 to 100 ppm, measured in the dark and zero gate-bias conditions. (e) Linear fitting of the gas-sensing response vs. gas concentration. (f) Selective sensitivity of the 8 layers ReS_2-FET toward different VOC gases under the same sensing conditions; in the dark and zero gate-bias conditions.

(Reproduced from ref. [1], ACS Applied Materials &Interfaces, Submitted: June 2021).

The charge transfer of VOC gases to the ReS_2 surface was investigated using Kelvin probe force microscopy (KPFM) by estimating the surface potential of a ReS_2 device under different VOC gas exposure; acetone, methanol, ethanol and IPA, at room temperature, to verify the carrier doping behavior of VOC molecules as donor or acceptor. The work function difference between the ReS_2 (W_{ReS2}) and the AFM tip (W_{tip}) determines the surface potential, also known as potential contact difference (CPD). In this regard, the CPD signals measured in numerous sections of the ReS_2 reflect their respective work functions.[14,15] **Figure 4-5**a and **4-5**b show the KPFM image of the ReS_2 device and its surface potential profile before VOC gas exposure, respectively (measured along the green line, whereby the surface potential is measured from that of SiO_2 surface). **Figures 4-5**c**, 4-5**d**, 4-5**e, and **4-5**f display the surface potential profile after acetone, methanol,

ethanol and IPA exposure, respectively. The surface potential of the ReS_2 increases from 100 to 175 mV (after acetone exposure) and from 100 to 120 mV (after methanol exposure). These indicate that the difference between the conduction band and the Fermi level of the ReS_2 will increase (means less *n*-type behavior), with which acetone demonstrated stronger electron acceptor capability than methanol.

Meanwhile, the surface potential of the ReS_2 upon ethanol exposure decreases from 100 to 70 mV, which suggests that the Fermi level of ReS_2 is shifted toward the conduction band (means more *n*-type behavior). These changes further reveal that ethanol acts as an electron donor; the electrons were transferred from ethanol to ReS_2 to reduce the *n*-type channel resistance. Alternatively, the surface potential upon IPA exposure remains unchanged because there is no charge transfer to happen, which mean that the device is insensitive to IPA. These differences are suggested to be related to the different value of electron affinity between ReS_2 and each molecule, in which some molecules can act as electron acceptor or electron donor.

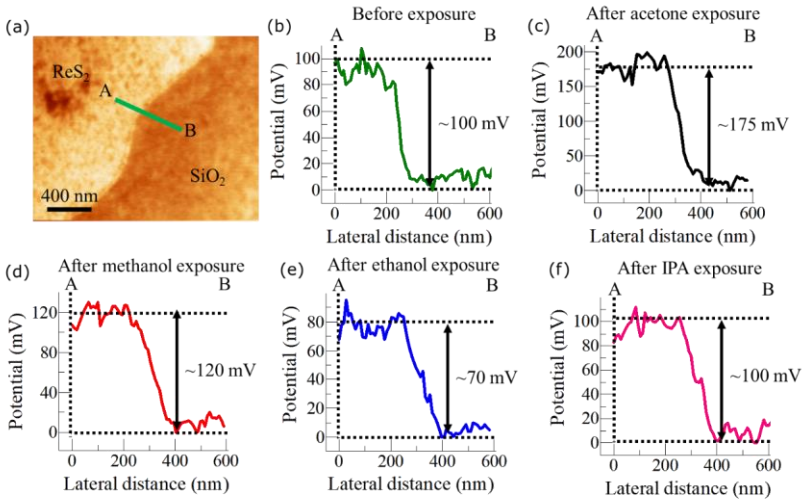

Figure 4-5. (a) Kelvin probe force microscopy (KPFM) image and (b) its potential surface profile of the device before exposure. KPFM potential profile after VOC gases; (c) acetone, (d) methanol, (e) ethanol and (f) IPA exposure at room temperature.

(Reproduced from ref. [1], ACS Applied Materials &Interfaces, Submitted: June 2021).

To further explore the sensing mechanism of these VOC gases, the sensing process was simulated by the first-principles calculations based on density functional theory (DFT). The influence of vdW forces between the molecules and the ReS_2 nanoflakes was considered. Different orientations and initial positions of the gas molecules were also considered to determine the optimized gas orientation on ReS_2. In this study, the adsorption energy of gas molecules adsorbed on the ReS_2 nanoflakes is calculated using the following equation.

$$E_{\text{adsorption\_energy}} = E_{\text{ReS2+gasmolecule}} - E_{\text{ReS2}} - E_{\text{gasmolecule}} \quad (4-3)$$

$E_{\text{ReS2+gasmolecule}}$, E_{ReS2} and $E_{\text{gasmolecule}}$ represent the total energy of the ReS_2 layer with an adsorbed gas molecule, ReS_2 layer and gas molecule, respectively (see Supplementary Data Section, for the DFT calculation details). The simulation results of adsorption energy and the geometrically optimized crystal structure of ReS_2 upon the adsorption of gas molecules are summarized in **Figure 4-6** and **Table 4-1**. It is found that the adsorption energy of acetone, methanol, ethanol and IPA adsorbed on ReS_2 is –0.4375, –0.3025, –0.3615 and –0.4192 eV/system, respectively.

Based on the Bader charge analysis, the value of charge transfer between the ReS_2 layer and the adsorbed gas molecules was further calculated.[16] For a clearer demonstration, **Figure 4-7** shows the charge density difference images for the ReS_2 layer with acetone gas adsorption with which calculated by the formula:

$$\Delta\rho = \rho_{\text{ReS2+acetone}} - \rho_{\text{acetone}} - \rho_{\text{ReS2}} \quad (4-4)$$

where $\rho_{ReS2+acetone}$, $\rho_{acetone}$ and ρ_{ReS2} are the charge densities of the ReS_2-adsorbed acetone, isolated acetone and ReS_2, respectively. The dark-blue (yellow) distribution represents charge depletion (accumulation) and the total charge distributed in the acetone molecule is negative on average. **Table 4-2** summarizes the calculated results, in which a negative ΔQ_b represents an electron charge transfer from ReS_2 to a gas molecule. To highlight, acetone and methanol behave as electron acceptors, accepting 0.012*e* (acetone) and 0.008*e* (methanol) from the ReS_2 layer. Besides, the ReS_2 device displays insensitive sensing toward IPA (0.000*e*). These results further conform to the initial gas-sensing measurement in **Figure 4-4**. Meanwhile, for ethanol, the value of ΔQ_b is too small due to the limitation of the resolution of the DFT calculation.

Table 4-1. Adsorption energy of VOCs gas molecules with different orientation adsorbed on ReS_2. Flat orientation has the lowest adsorption energy upon each gas adsorption, suggesting flat-orientation is the most stable configurations in the DFT calculations.

Gas orientation	**Adsorption energy, eV/system**
Acetone-bottom	–0.2686
Acetone-flat	**–0.4375**
Acetone-top	–0.3715
Methanol-bottom	–0.2524
Methanol-flat	**–0.3025**
Methanol-top	–0.2497
Ethanol-bottom	–0.3518
Ethanol-flat	**–0.3615**
Ethanol-top	–0.2165
IPA-bottom	–0.2567
IPA-flat	**–0.4192**
IPA-top	–0.3518

(Reproduced from ref. [1], ACS Applied Materials &Interfaces, Submitted: June 2021).

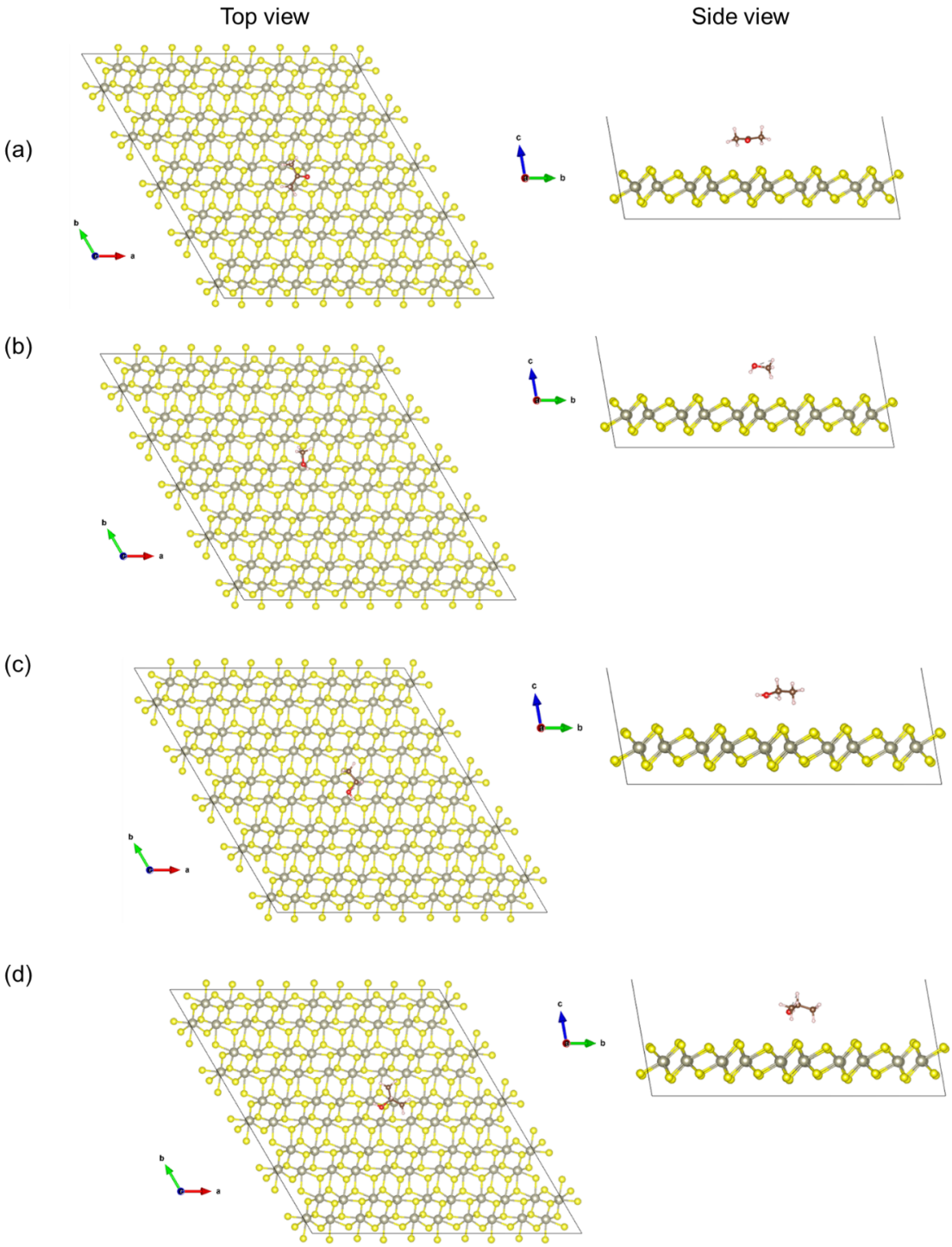

Figure 4-6. The geometrically optimized crystal structure of ReS_2 layer with an adsorbed (a) acetone, (b) methanol, (c) ethanol, and (d) IPA molecules from a top view and side view (flat orientation).

(Reproduced from ref. [1], ACS Applied Materials &Interfaces, Submitted: June 2021).

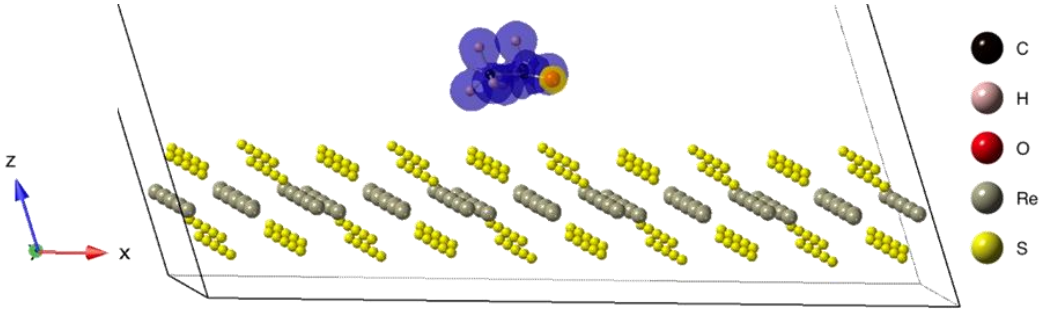

Figure 4-7. Charge density difference of the ReS_2 + acetone system (side views). The electron charge depletion is represented by dark-blue color. The iso-surface is set to 5×10^{-1} e/ $Å^3$.

(Reproduced from ref. [1], ACS Applied Materials &Interfaces, Submitted: June 2021).

Table 4-2. The Bader charge analysis value (ΔQ_b) of VOC gas molecules adsorbed on ReS_2.

Gas molecule	**Gas Orientation**	**ΔQ_b (e)**
Acetone	Acetone-flat	–0.012
Ethanol	Ethanol-flat	0.000
Methanol	Methanol-flat	–0.008
IPA	IPA-flat	0.000

(Reproduced from ref. [1], ACS Applied Materials &Interfaces, Submitted: June 2021).

As mentioned above, the sensing behavior of the device is still difficult to selectively detect specific target gas in VOC mixtures. For instance, C_{gas} dependence of S_{gas} for acetone and methanol exhibit slightly comparable values (**Figure 4-4)**, which is undesirable for specific VOCs gas detection. However, the sensing response of ReS_2-FET by light illumination is marked differently. The sensing measurements of **Figure 4-4** were repeated with the illumination of light to the ReS_2-FET sensor device under 100 ppm VOC gas exposure, which enables to induce a different response to adsorption of different gas species. In our experiment in VOC gas-sensing shown in **Figures 4-8**a and **4-8**b, it is demonstrated that the response is positive in both cases of acetone and methanol while it is negative in the case of ethanol. Here, the most important feature is that acetone and

methanol will be distinguished by changing the wavelength at positive V_g. As shown in **Figures 4-8**a and **4-8**b, the response to acetone was enhanced as the wavelength was increased from λ = 340 nm to λ = 650 nm, while it was decreased in the case of methanol. Also, the difference between acetone and methanol is much more enhanced by increasing the gate bias from V_G = 0 to 40 V, as shown in **Figure 4-8b**, which also contributes to distinguishing acetone and methanol.

Alternatively, in ethanol, the sensing behavior under light illumination is also different from that in acetone and methanol. The strength of response under the light illumination is enhanced under the increased wavelength, but the largest response of –87% is given under the dark condition, as shown in **Figure 4-8**c. Also, these differences can be modulated by the gate-bias condition, in which +40 V and –40 V back-gate bias were further enhanced the sensing selectivity toward acetone and ethanol, respectively, with a sensitivity value of 4.34% ppm^{-1} (acetone, **Figure 4-8**d, **4-8**e and **4-8**f) and –0.85% ppm^{-1} (ethanol, **Figure 4-9**). **Figure 4-8**e shows an anti-interference of acetone sensor performance in a complex atmosphere (selective detection of acetone vapor in a mixed gas measured under V_G= +40V and λ = 650 nm light illumination). The response toward methanol, ethanol, and IPA was much less and negligible than toward acetone. In this manner, the ReS_2-FET sensor can enhance the selectivity in chemical sensing performance by light illumination by taking advantage of different responses to light illumination, which is characteristic of each molecule.

Overall, the sensing mechanisms of ethanol and acetone sensors are illustrated in **Figures 4-10**a and **4-10**b, respectively. As the sensor device is exposed to ethanol shown in **Figure 4-10**a, ethanol as an electron donor will be adsorbed on the ReS_2 surface. Thus, electrons were transferred from ethanol to ReS_2, which is causing electron doping in ReS_2.

Subsequently, the sensor resistance is decreased. Then, when the negative gate bias is applied, the concentration of the capacitively induced carriers in ReS_2 would largely decrease. This will induce fewer electrons to accumulate on the ReS_2 surface, responsible for enhancing the sensor's gas-sensing performance toward ethanol.

Meanwhile, in the case of acetone shown in **Figure 4-10**b, acetone as an electron acceptor will be adsorbed onto the ReS_2 surface, thus transferring the electrons from ReS_2 to acetone. This will cause electron depletion in ReS_2 with which increased the sensor resistance. When light illumination and back-gate biasing are applied, the concentration of the photogenerated carriers and capacitively induced carriers in ReS_2 would largely increase because of the excellent photosensitivity and transistor properties of ReS_2, respectively. By applying light, more electrons will be induced to accumulate on the ReS_2 surface and thus get captured by acetone, whereby the electron transfer rates to acetone are higher than the electron-hole pair generation by the incident light. This effect is considered to cause more enhanced sensitivity by the larger photocurrent in acetone, as shown in **Figure 4-3**c. Meanwhile, in methanol, it is speculated that the wavelength dependence of the photocurrent, as shown in **Figure 4-3**c, was retained even when it is exposed to methanol. However, the precise mechanism of different responses by light illumination should also be understood by considering the efficiency of electron-hole pair generation and their recombination, trapping of generated carriers by trapping site in the channel or the interface of the channel and substrate, the energy level of the trapping sites, de-trapping of carriers by biasing and heating by light. So many factors will be included in the consideration, and therefore, the precise mechanism should be carefully investigated in further detailed experiments from multiple viewpoints.

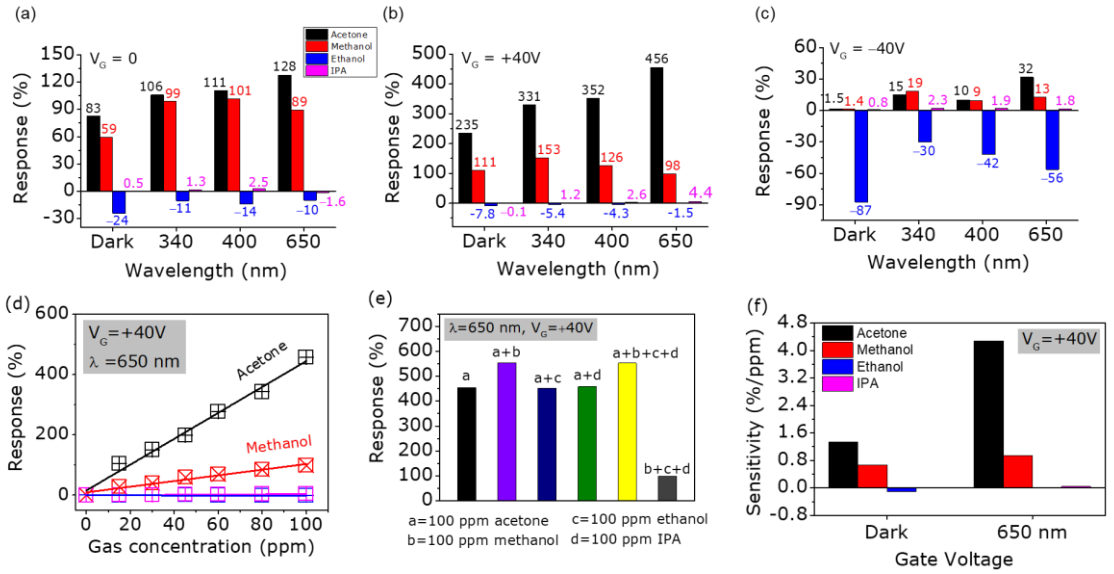

Figure 4-8. The gas-sensing performance of 8 layers ReS_2-FET sensor toward 100 ppm VOC gases in the dark and under light illumination with different wavelengths, as well as different gate bias; (a) V_G = 0, (b) V_G = +40 V and (c) V_G = –40 V. (d) Linear fitting of the ReS_2-FET response vs. gas concentration under V_G = +40V and λ = 650 nm light illumination. Gas concentration ranging from 0 to 100 ppm. (e) Selective detection of acetone vapor in a mixed gas measured under V_G = +40V and λ = 650 nm light illumination. (f) Gas sensor sensitivity for different VOC gases under V_G = +40V and λ = 650 nm light illumination.

(Reproduced from ref. [1], ACS Applied Materials &Interfaces, Submitted: June 2021).

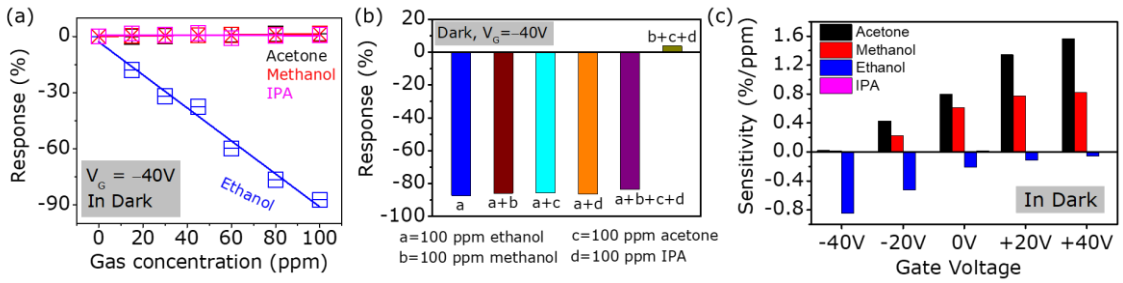

Figure 4-9. (a) Linear fitting of the ReS_2-FET response vs. gas concentration in dark and –40V gate bias conditions. (b) Selective detection of ethanol vapor in a mixed gas measured in dark and –40 V gate bias conditions. (c) Gas sensor sensitivity for different VOC gases under dark environment and various gate bias.

(Reproduced from ref. [1], ACS Applied Materials &Interfaces, Submitted: June 2021).

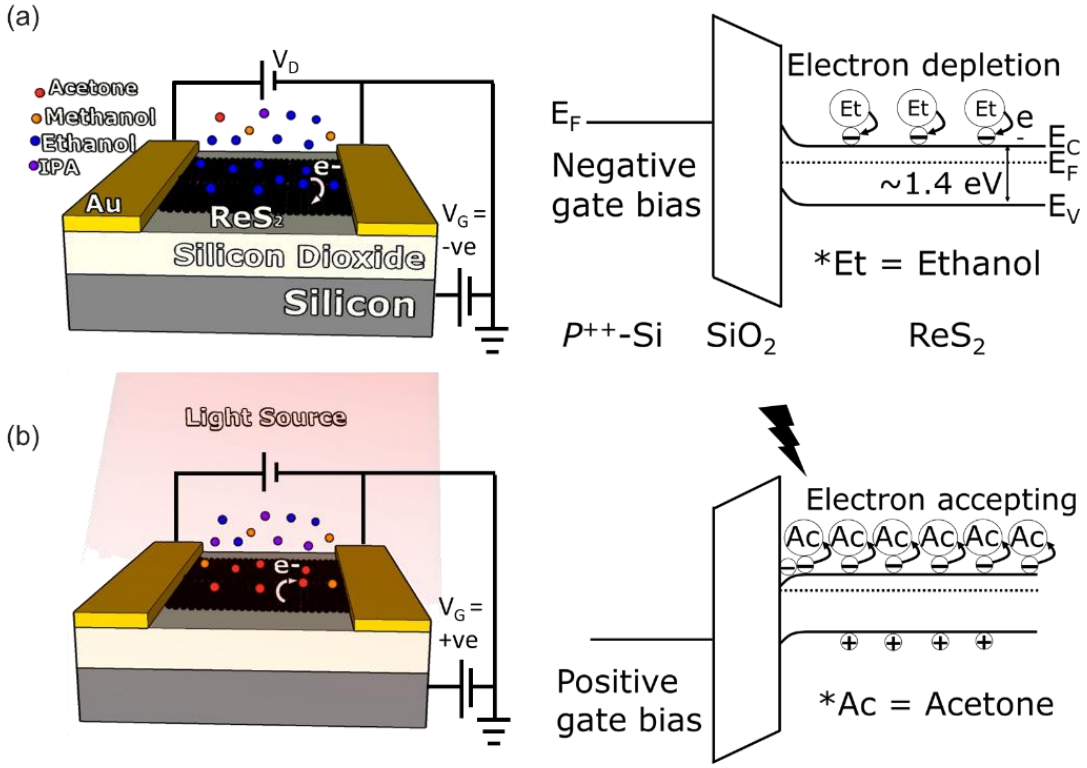

Figure 4-10. Schematic diagram and band diagram of the sensing mechanism of ReS_2-FET sensor selectively detected (a) ethanol in dark and –40 V gate bias conditions, and (b) acetone under +40 V gate bias and λ=650 nm light illumination.

(Reproduced from ref. [1], ACS Applied Materials &Interfaces, Submitted: June 2021).

4.3.3. Stability and durability properties of ReS_2-FET based VOCs gas sensor

Another vital criterion for practical gas sensors operation is long-term stability and durability. Here, the sensing measurements were repeated 7 times within 30 days, and after each measurement, the gas chamber was flushed with nitrogen gas for a few minutes to recover the sensor to the initial condition. The results show that the response is unchanged even after 30 days (**Figure 4-11**). This indicates that the devices operated under specific sensing operations possess long-term stability. Also, it presents negligible performance degradation than other transistor-based sensors such as black phosphorus transistor-based gas sensors and others.[17] **Table 4-3** and **4-4** lists the gas performance

for various 2D materials-based gas sensors detecting acetone and ethanol, showing that our device outperforms most of these reported works, especially on the selectivity matter, which focuses on using a single-device based 2D material FET. In this regard, a single device of ReS_2-FETs operated under specific sensing conditions can further progress the gas sensor toward versatile and highly selective detection of VOC gases.

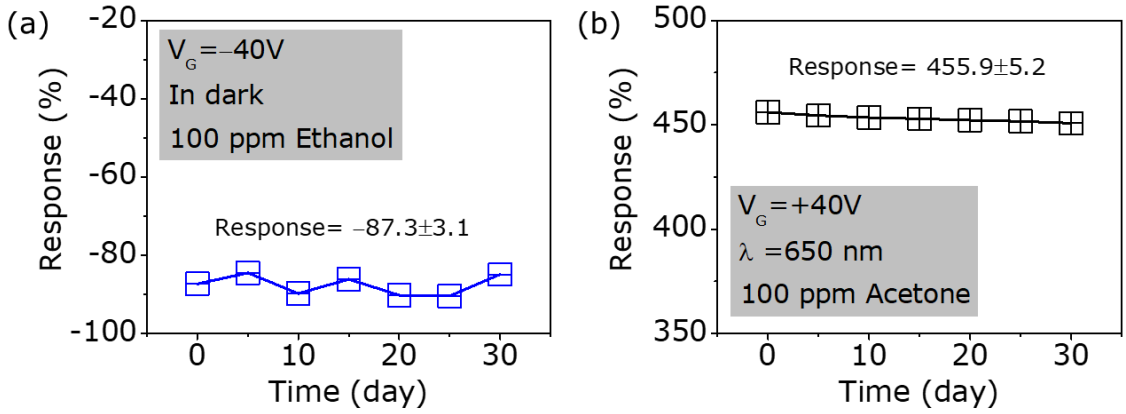

Figure 4-11. The **s**tability of the gate-bias and light-assisted ReS_2-FET gas sensor to (a) 100 ppm ethanol and (b) 100 ppm acetone within 30 days.

(Reproduced from ref. [1], ACS Applied Materials &Interfaces, Submitted: June 2021).

Table 4-3. Compilation of acetone sensing performance results for a variety of 2D materials-based gas sensors.

Sensing channel	Response (%)	Sensitivity (% ppm^{-1})	Light wavelength	Gate biasing	Temperature (°C)	Environment	Ref.
rGO/CuO/ZnO composite	9.4 (10 ppm) *ii	-	-	-	340	Air	[18] 2014
MoS_2 layers	15 (1000 ppm) *i	-	-	-	25	N_2	[19] 2014
rGO/SnO_2 composite	2.19 (10 ppm) *i	-	-	-	25	Air	[20] 2015
rGO/$CdFe_2O_4$ composite	2 (0.01 ppm) *ii	-	-	-	270	Air	[21] 2015
Co_3O_4 nanosheets	11.4 (100 ppm) *ii	-	-	-	150	Air, RH 50%	[22] 2015
Graphene/ZnO composite	13.3 (100 ppm) *ii	-	-	-	280	Air	[23] 2016
Co_3O_4 nanosheets	6.1 (100 ppm) *ii	-	-	-	160	Air	[24] 2016
N-doped rGO/TiO_2 composite	19 (1000 ppm) *iii	-	-	-	270	Air	[25] 2016
Graphene layer	2.28% (900 ppb) *i	-	-	-	25	N_2	[26] 2017
rGO/α-Fe_2O_3 nanofibers	8.9 (100 ppm) *ii	-	-	-	375	Air, RH20%	[27] 2017
rGO/α-Fe_2O_3 composite	13.9 (100 ppm) *ii	-	-	-	225	Air, RH30%	[28] 2017
rGO/In_2O_3 composite	85 (25 ppm) *i	-	-	-	175	Air, RH53%	[29] 2017
Au-loaded MoS_2 layers	15 (1000 ppm) *i	-	-	-	25	N_2	[30] 2017
Sn-doped ZnO nanosheets	5.556 (200 ppm) *ii	-	-	-	320	Dry air	[31] 2017
$Ti_3C_2T_x$ (MXene) nanosheets	0.0075 (100 ppm) *i	-	-	-	25	Air	[32] 2017
GO/SnO_2/TiO_2 composite	12.7 (1 ppm) *ii	-	-	-	200	Air, RH35~95%	[33] 2018

GO/WO_3 nanofibers	35.9 (100 ppm) *ii	-	-	-	375	Air	[34] 2018
Gd-doped rGO/WO_3 composite	24 (20 ppm) *ii	-	-	-	200	Air	[35] 2018
Pt-loaded rGO/WO_3 composite	12.2 (10 ppm) *ii	-	-	-	200	Air	[36] 2018
WO_3/SnO_2 nanosheets	12.1 (10 ppm) *ii	-	-	-	260	Air	[37] 2018
$Ti_3C_2T_x$ (MXene) layers	0.97 (100 ppm) *i	-	-	-	25	N_2	[38] 2018
$Ti_3C_2T_x$ (MXene) layers	3.6 (5 ppm) *i	-	-	-	25	N_2	[39] 2018
g-C_3N_4/WO_3 nanosheets	35 (100 ppm) *ii	-	-	-	340	Air	[40] 2019
ReS_2	104.8 (100 ppm) *i	4.3	λ=650 nm, 8.4 mW/cm^2	+40 V	25	Air, RH50%	This work

(Reproduced from ref. [1], ACS Applied Materials &Interfaces, Submitted: June 2021).

Table 4-4. Compilation of ethanol sensing performance results for a variety of 2D materials-based gas sensors.

Sensing channel	**Response (%)**	**Sensitivity (% ppm^{-1})**	**Light wavelength**	**Gate biasing**	**Temperature (°C)**	**Environment**	**Ref.**
SnO_2@MoS_2	160 (500 ppm) *ii	-	-	-	280	Air	[41] 2015
ZnO@Graphene	8.5 (10 ppm) *i	-	-	-	~400	Air	[42] 2015
rGO/SnO_2	28.7 (50 ppm) *i	-	-	-	170	Air	[43] 2016
PVP/TiS_2	6800 (18 ppm) *iv	-	-	-	25	Air, RH70%	[44] 2019
WS_2/GONRs	126.5 (1 ppm) *iii	-	-	-	25	Air, RH40%	[45] 2020
ReS_2	–87.3 (100 ppm) *i	–0.85% ppm^{-1}	-	–40 V	25	Air	This work

(Reproduced from ref. [1], ACS Applied Materials &Interfaces, Submitted: June 2021).

The symbol above represents as follow:

Response calculated by

*i : $\frac{\Delta R}{R_O} \times 100\%$, *ii : $\frac{R_g}{R_O} or \frac{R_g}{R_O}$, *iii : $\frac{\Delta I}{I_O} \times 100\%$, *iv : $\frac{I_g}{I_O} or \frac{I_g}{I_O}$

(The content in this chapter is reproduced from [1], ACS Applied Materials &Interfaces, Submitted: June 2021).

4.4. Conclusion

We have developed selective and sensitive detection of VOC gases using a single device of 2D ReS_2-FET with an enhanced selectivity of gas species by light illumination. By using the fabricated device, we have investigated the detection of VOC gases of acetone, methanol and IPA. Selective and sensitive detection (4.3% ppm^{-1}) of acetone gas was demonstrated with the aid of λ = 650 nm light illumination and +40V gate bias to distinguish between different VOC gases. Meanwhile, selective and sensitivity of ethanol sensing (–0.85% ppm^{-1}) were achieved under dark conditions. With the illumination of light, it is proved that the selectivity of VOC gas species in our device is improved by the different behavior of the response current to the gas molecule adsorption to the ReS_2 surface under illumination of light with different wavelengths. For example, without light illumination with different wavelengths, it was not easy to distinguish between acetone and methanol by our ReS_2-FET sensor device. Besides, stable device operation and long-term device stability within a long period allowed the sensor to be used in real-time applications. In the practical use of chemical sensor applications, it must detect an almost infinite number of gas species by a finite number of sensor devices, and for this purpose, building big data and analysis by artificial intelligence is supposed to become important. In this regard, increasing the number of independent/input parameters in the sensing process, such as the light intensity and wavelength, will become important for extracting each molecule's characteristic properties. By accumulating the response tendency of each gas molecules against these input parameters, the gas molecule as well as gas concentration could be detected. The device concept presented in this work established the first step of long-term gas sensor development toward high selectivity gas

detection, enabling us to enlarge the big data accumulation both in quality and quantity for detecting the almost infinite number of molecules around us.

4.5. Supplementary data

4.5.1. Influence of ReS_2 thickness on VOCs gas sensing response

In this study, three different thickness of 6 layers, 8 layers, and 11 layers ReS_2-FETs were prepared to clarify the role of ReS_2 thickness on the VOCs gas sensing performance. Herein, **Figure S4-1** show the response of ReS_2-FET based VOCs gas sensor with different ReS_2 thicknesses. These were studied under different sensing measurement condition: gate bias tunability and light illumination. The VOCs gas concentration was fixed at 100 ppm. Looking at these figures, the sensing response for 8 layers ReS_2-FET demonstrated comparable data as compared to 11 layers ReS_2-FET. For thin flakes like 1-10 nm thick ReS_2, full flake will get depleted/accumulated under negative/positive gate bias. However, for thicker flake only few layers near to SiO_2 interface will get affect so there will be non-uniform photocarrier generation in thicker flake under light illumination and under gate field. As the flake thickness of the device for the experiment is within 10 nm, both the interface and channel effect under gate bias need to be discussed.

In addition, as the ReS_2 thickness increased, the charge carrier density increased due to its intrinsic properties, whereas more photo-absorption will take place as ReS_2 is direct band-gap material. However, there might have non-uniform carriers accumulation/depletion under gate-induced effect and non-uniform carriers generation under light illumination for thicker flake. Meanwhile, for gas sensing response, high surface-to-volume ratio is highly required. Therefore, there was a trade-off relation of

ReS_2 thickness and surface area-to-volume ratio for gas sensing response phenomena under a light illumination sensing operation. These results suggested that the optimal sensing response toward VOCs gas was achieved starting from 8 layers ReS_2-FET operated under a specific sensing operation.

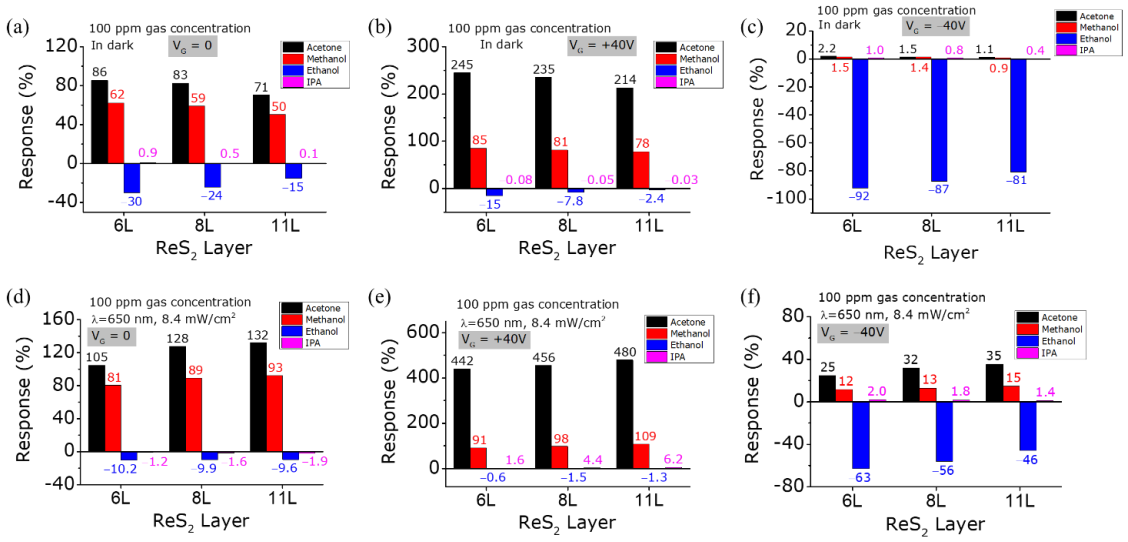

Figure S4-1. Sensing response vs. VOCs gas concentration for 6, 8, and 11 layers ReS_2-FET under different sensing measurement; (a) in dark and V_G = 0, (b) in dark and V_G = +40V, (c) in dark and V_G = –40V, (d) λ= 650 nm, 8.4 mW/cm^2 and V_G = 0, (e) λ= 650 nm, 8.4 mW/cm^2 and V_G = +40V, and (f) λ= 650 nm, 8.4 mW/cm^2 and V_G = –40V.

(Reproduced from ref. [1], ACS Applied Materials &Interfaces, Submitted: June 2021).

4.5.2. Influence of light intensity on VOCs gas sensing response

Another set of VOCs gas sensing measurement were also performed to examine the dependence of light intensity on the device sensing performance. **Figure S4-2** displays the sensing response of the 8 layers ReS_2-FET sensor toward 100 ppm VOCs gases in the dark and under 650 nm light illumination with different light intensity (0.5, 1.6, 5.6, 8.4, and 12.0 mW/cm^2).

The sensing response was significantly increased as the light intensity increased from 0 to 8.4 mW/cm^2. As the light intensity was further increased to 12 mW/cm^2, the

sensing response only displays a slightly increment, in which the light intensity of 8.4 mW/cm^2 is sufficient to be used in the gas sensing measurement operated under light illumination. This observation could be due to only carriers in few-layer thickness on the surface will respond to the gas molecules when the light interaction reaches beyond optimal value creating non-uniform photocarriers generation. Besides, based on **Figure 4-3**c, the phenomenon could also be explained that under light illumination, the carrier concentration in ReS_2 would largely increase due to the electron-hole pair generation. Thus, more electrons transferred from ReS_2 to oxidizing VOCs gases in company with the increase of the light intensity, which accounts for the substantial light enhancement of the gas sensing performance.

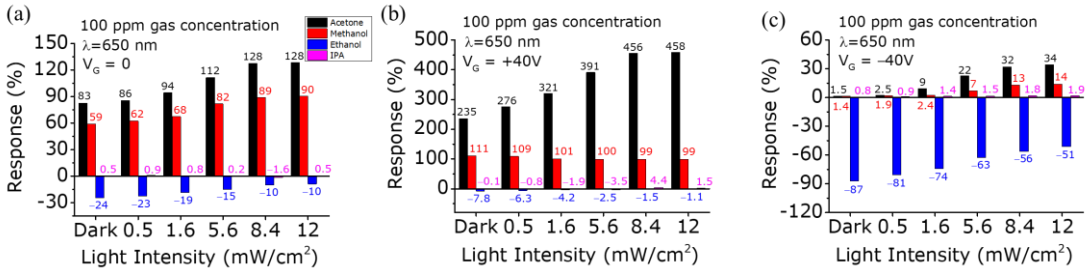

Figure S4-2. Gas sensing performance of 8 layers ReS_2-FET sensor toward 100 ppm VOCs gases in the dark and under 650 nm light illumination with different light intensity, as well as different gate bias; (a) V_G = 0, (b) V_G = +40 V, and V_G = –40 V.

(Reproduced from ref. [1], ACS Applied Materials &Interfaces, Submitted: June 2021).

References

[1] A. Zulkefli, B. Mukherjee, R. Sahara, R. Hayakawa, T. Iwasaki, Y. Wakayama, S. Nakaharai, *ACS Applied Materials & Interfaces* **2021**, *Submitted*.

[2] G. Kresse, J. Furthmüller, *Comput. Mater. Sci.* **1996**, *6*, 15.

[3] D. Joubert, *Phys. Rev. B - Condens. Matter Mater. Phys.* **1999**, *59*, 1758.

[4] P. E. Blöchl, *Phys. Rev. B* **1994**, *50*, 17953.

[5] J. P. Perdew, K. Burke, M. Ernzerhof, *Phys. Rev. Lett.* **1996**, *77*, 3865.

[6] T. Bučko, S. Lebègue, J. G. Ángyán, J. Hafner, *J. Chem. Phys.* **2014**, *141*.

[7] K. Momma, F. Izumi, *J. Appl. Crystallogr.* **2011**, *44*, 1272.

[8] A. McCreary, J. R. Simpson, Y. Wang, D. Rhodes, K. Fujisawa, L. Balicas, M. Dubey, V. H. Crespi, M. Terrones, A. R. Hight Walker, *Nano Lett.* **2017**, *17*, 5897.

[9] N. R. Pradhan, A. McCreary, D. Rhodes, Z. Lu, S. Feng, E. Manousakis, D. Smirnov, R. Namburu, M. Dubey, A. R. Hight Walker, H. Terrones, M. Terrones, V. Dobrosavljevic, L. Balicas, *Nano Lett.* **2015**, *15*, 8377.

[10] E. Liu, M. Long, J. Zeng, W. Luo, Y. Wang, Y. Pan, W. Zhou, B. Wang, W. Hu, Z. Ni, Y. You, X. Zhang, S. Qin, Y. Shi, K. Watanabe, T. Taniguchi, H. Yuan, H. Y. Hwang, Y. Cui, F. Miao, D. Xing, *Adv. Funct. Mater.* **2016**, *26*, 1938.

[11] M. Hasegawa, T. Shimakura, *J. Appl. Phys.* **2010**, *107*, 084107.

[12] L. D. Bharatula, M. B. Erande, I. S. Mulla, C. S. Rout, D. J. Late, *RSC Adv.* **2016**, *6*, 105421.

[13] B. J. Liu, X. Wang, Q. Peng, *Adv. Mater.* **2005**, *17*, 764.

[14] Z. Feng, B. Chen, S. Qian, L. Xu, L. Feng, Y. Yu, R. Zhang, J. Chen, Q. Li, Q. Li, C. Sun, H. Zhang, J. Liu, W. Pang, D. Zhang, *2D Mater.* **2016**, *3*, 1.

[15] J. Zeng, Y. Niu, Y. Gong, Q. Wang, H. Li, A. Umar, N. F. de Rooij, G. Zhou, Y.

Wang, *ACS sensors* **2020**, *5*, 3172.

[16] G. Henkelman, A. Arnaldsson, H. Jónsson, *Comput. Mater. Sci.* **2006**, *36*, 354.

[17] S. Yang, C. Jiang, S. Wei, *Appl. Phys. Rev.* **2017**, *4*, 021304.

[18] C. Wang, J. Zhu, S. Liang, H. Bi, Q. Han, X. Liu, *J. Mater. Chem. A* **2014**, *2*, 18635.

[19] J. Kim, H. Yoo, H. O. Choi, H. Jung, *Nano Lett.* **2014**, *14*, 5941.

[20] D. Zhang, A. Liu, H. Chang, B. Xia, *RSC Adv.* **2015**, *5*, 3016.

[21] T. Hu, X. Chu, F. Gao, Y. Dong, W. Sun, L. Bai, *Mater. Sci. Semicond. Process.* **2015**, *34*, 146.

[22] Z. Zhang, Z. Wen, L. Zhu, *RSC Adv.* **2015**, *5*, 59976.

[23] H. Zhang, Y. Cen, Y. Du, S. Ruan, *Sensors* **2016**, *16*, 1876.

[24] Y. Lin, H. Ji, Z. Shen, Q. Jia, D. Wang, *J. Mater. Sci. Mater. Electron.* **2016**, *27*, 2086.

[25] W. Yan, Q. Zhou, X. Chen, X. Huang, Y. Wu, *Sensors Actuators B. Chem.* **2016**, *230*, 761.

[26] C. M. Yang, T. C. Chen, Y. C. Yang, M. C. Hsiao, M. Meyyappan, C. S. Lai, *Vacuum* **2017**, *140*, 89.

[27] L. Guo, X. Kou, M. Ding, C. Wang, L. Dong, H. Zhang, C. Feng, Y. Sun, Y. Gao, P. Sun, G. Lu, *Sensors Actuators B. Chem.* **2017**, *244*, 233.

[28] B. Zhang, J. Liu, X. Cui, Y. Wang, Y. Gao, P. Sun, F. Liu, K. Shimanoe, N. Yamazoe, G. Lu, *Sensors Actuators B. Chem.* **2017**, *241*, 904.

[29] R. K. Mishra, G. Murali, T. Kim, J. H. Kim, Y. J. Lim, B. Kim, P. P. Sahay, S. H. Lee, *RSC Adv.* **2017**, *7*, 38714.

[30] S. Y. Cho, H. J. Koh, H. W. Yoo, J. S. Kim, H. T. Jung, *ACS Sensors* **2017**, *2*, 183.

[31] Y. Al-hadeethi, A. Umar, R. Kumar, S. H. Kim, X. Zhang, *Ceram. Int.* **2017**, *43*,

2418.

[32] E. Lee, A. VahidMohammadi, B. C. Prorok, Y. S. Yoon, M. Beidaghi, D.-J. Kim, *ACS Appl. Mater. Interfaces* **2017**, *9*, 37184.

[33] R. Kalidoss, S. Umapathy, Y. Sivalingam, *Appl. Surf. Sci.* **2018**, *449*, 677.

[34] J. Zhang, H. Lu, C. Yan, Z. Yang, G. Zhu, J. Gao, F. Yin, C. Wang, *Sensors Actuators B. Chem.* **2018**, *264*, 128.

[35] J. Kaur, K. Anand, A. Kaur, R. C. Singh, *Sensors Actuators B. Chem.* **2018**, *258*, 1022.

[36] L. Chen, L. Huang, Y. Lin, L. Sai, Q. Chang, W. Shi, Q. Chen, *Sensors Actuators B. Chem.* **2018**, *255*, 1482.

[37] M. Yin, Y. Yao, H. Fan, S. Liu, *J. Alloys Compd.* **2018**, *736*, 322.

[38] S. Cho, B. Anasori, C. Kim, Y. Choi, J. Kim, Y. Gogotsi, *ACS Nano* **2018**, *12*, 986.

[39] W. Yuan, *J. Mater. Chem. A* **2018**, *6*, 18116.

[40] D. Wang, S. Huang, H. Li, A. Chen, P. Wang, J. Yang, *Sensors Actuators B. Chem.* **2019**, *282*, 961.

[41] H. Yan, P. Song, S. Zhang, Z. Yang, Q. Wang, *RSC Adv.* **2015**, *5*, 79593.

[42] S. Liang, J. Zhu, J. Ding, H. Bi, P. Yao, Q. Han, X. Wang, *Appl. Surf. Sci.* **2015**, *357*, 1593.

[43] S. Xu, F. Sun, Z. Pan, C. Huang, S. Yang, J. Long, Y. Chen, *ACS Appl. Mater. Interfaces* **2016**, *8*, 3428.

[44] S. H. Hosseini-Shokouh, S. Fardindoost, A. I. Zad, *ChemistrySelect* **2019**, *4*, 6662.

[45] H. Ahmadvand, A. Iraji zad, R. Mohammadpour, S. H. Hosseini-Shokouh, E. Asadian, *Sci. Rep.* **2020**, *10*, 1.

Chapter 5
Summary and future works

5.1. Summary of dissertation

In summary, this dissertation has provided a new way to develop highly selective and sensitive gas sensor using a single device sensor of ReS_2-FET by utilizing the effective response of ReS_2 to light illumination as well as gate biasing. Additionally, a better understanding of the sensor device operation by a single device ReS_2-FET was established.

In chapter 2, the humidity sensing performance and mechanism of few-layer-thick ReS_2-FET under gate bias operation was investigated. This chapter employed gate biasing operation to design high-quality ReS_2-FET based humidity sensors, whereby the sensing performance and underlying mechanism were discussed with respect to the gate bias operation. Consequently, a negative gate bias exhibits the sensor response, exceeding 90% mainly in the low relative humidity (RH) range. Meanwhile, the threshold voltage change was discovered to be a superior sensing parameter to achieve a broad monitoring of RH range with high response and sensitivity. The approach obtained a practical sensitivity of 0.4 V per 1% RH, which exceed a majority of previous studies with the pristine 2D materials. Besides, our devices display reversible adsorption–desorption and long-term stability operations even after a one-month period. This suggests the sensor capacity to function in real-time applications with a short response and recovery times. These outcomes offer support in the development of adaptable tunable humidity sensors.

In chapter 3, we focused on the investigation of the oxygen gas sensor performance and mechanism of few-layer-thick ReS_2-FET under both light illumination

and gate biasing. This combination sensing concept enhanced the device response over 100% at a 1% oxygen concentration; that is, the approach achieves a practical sensitivity of 0.01% ppm^{-1}, which have outperformed most of the reports available in the literature. Also, the fabricated devices exhibit long-term stability and stable operation even under humid conditions, indicating the ability of the sensor device to operate in a real-time application, which contribute to the development of versatile tunable oxygen sensors based on TMDC FETs.

In chapter 4, we have developed selective and sensitive detection of VOC gases using a single device of 2D ReS_2-FET with an enhanced selectivity of gas species by light illumination. By using the fabricated device, we have investigated the detection of VOC gases of acetone, methanol and IPA. Selective and sensitive detection (4.3% ppm^{-1}) of acetone gas was demonstrated with the aid of λ = 650 nm light illumination and +40V gate bias to distinguish between different VOC gases. Meanwhile, selective and sensitivity of ethanol sensing (–0.85% ppm^{-1}) were achieved under dark conditions. With the illumination of light, it is proved that the selectivity of VOC gas species in our device is improved by the different behavior of the response current to the gas molecule adsorption to the ReS_2 surface under illumination of light with different wavelengths. For example, without light illumination with different wavelengths, it was not easy to distinguish between acetone and methanol by our ReS_2-FET sensor device. Besides, stable device operation and long-term device stability within a long period allowed the sensor to be used in real-time applications. In the practical use of chemical sensor applications, it must detect an almost infinite number of gas species by a finite number of sensor devices, and for this purpose, building big data and analysis by artificial intelligence is supposed to become important. In this regard, increasing the number of

independent parameters in the sensing process, such as the light intensity and wavelength, will become important for extracting each molecule's characteristic properties. The device concept presented in this work enables us to enlarge the big data both in quality and quantity for detecting the almost infinite number of molecules around us.

5.2. Future works

Highly sensitive and selective gas sensor based on ReS_2-FET has been presented and addressed in this study as well as in many high impact factor publications. Despite the advancement that has been made in this research, a number of future directions listed below, would bring an optimization on the current sensing performance of the developed gas sensor.

i) Detail analysis on gas-solid interaction

Although the sensing mechanism for humidity sensor (**chapter 2**), oxygen sensor (**chapter 3**), and VOC gas sensor (**chapter 4**) has been discussed, detail fundamental work on gas-solid interaction has yet to be investigated and verified. For instance, the precise mechanism of different response by light illumination should be understood by considering the efficiency of electron-hole pair generation and their recombination, trapping of generated carriers by trapping site in the channel or the interface of the channel and substrate, energy level of the trapping sites, de-trapping of carriers by gate biasing and also heating by the light, and so on. In this manner, there are so many factors should be included in the consideration and carefully investigate in the further detailed experiments from multiple viewpoints.

ii) High frequency FET gas sensing

While the Internet of Things (IoT) is on the rise, the 5G will improve IoT performance and reliability. In this manner, the development of high frequency FET is another route to be investigated for wireless networks of multifunctional high frequency electronics devices employing ReS_2 and other nanomaterials for being integrated in the new generation of unattended gas sensor networks.

Acknowledgment

First and foremost, I would like to express my heartfelt gratitude to my supervisor and co-supervisor, Professor Yutaka Wakayama and Dr. Shu Nakaharai for every bit of support, patience, guidance, assistance, they have provided since the first day I work in Quantum Device Engineering group (QDEG). Importantly, I want to thank them for giving me the second change that I thought will never come.

I would like to acknowledge The Kyushu-NIMS Joint Graduate School Program for the support in my doctoral study and made my PhD work possible. Also, thank you to former members of QDEG whom I considered as my mentor, Dr. Bablu Mukherjee and Dr. Takuya Iwasaki. They have shared and taught me a great deal about research in gas sensor, and material science, provided help for my publications and at the same time, becoming my good friends. I am also grateful for all scientist and staffs in QDEG, particularly; Ms. Remi Minoshima and Dr. Ryoma Hayakawa for their generous assistance during my doctoral study, as well as Dr. Ryoji Sahara from Research Center for Structural Materials (NIMS-Sengen). Also, thank you to my former lab/office mate; Dr. Nguy Tin Phan and Dr. Efi Dwi Indari for their kind help and guidance in many things during my doctoral study. It is truly appreciated. I would also like to give gratitude to all my best friends especially Dr. Abdillah Sani who support me a lot during this journey, for being a good listener and for always putting up with me.

Special thanks go to my entire family; my parents, sister, brother, the in-laws, for their continuous prayers, love, and supports. To my dearly loved children Tasnim, Rizq Iskandar, and Rizq Ilman for always being my motivation and driving force. Final acknowledgement is saved for my beloved wife and my very best friend in the world, Wan Nor Aina for the endless support, love, and encouragement. Thank you very much for letting me rekindles my dreams and for never stops having faith in me.

Tsukuba, June 2021

Mohd Amir bin ZULKEFLI

List of Publications

- **Zulkefli, A.**, Mukherjee, B., Iwasaki, T., Hayakawa, R., Nakaharai, S., & Wakayama, Y. (2021). Enhanced Selectivity in Volatile Organic Compound (VOCs) Gas Sensors Based on ReS_2-FETs under Light-Assisted and Gate-Bias Tunable Operation. (ACS Applied Materials & Interfaces, Under Review: June 2021).

- **Zulkefli, A.**, Mukherjee, B., Iwasaki, T., Hayakawa, R., Nakaharai, S., & Wakayama, Y. (2021). Gate-Bias Tunable Humidity Sensors based on Rhenium Disulfide Field-Effect Transistors. Japanese Journal of Applied Physics, 60(SB), SBBH01. https://doi.org/10.35848/1347-4065/abd2a0.

- **Zulkefli, A.**, Mukherjee, B., Iwasaki, T., Hayakawa, R., Nakaharai, S., & Wakayama, Y. (2020). Gate-Bias Assisted Humidity Sensor based on ReS_2 Field-Effect Transistors. Extended Abstract Solid State Devices and Materials, p. 559.

- **Zulkefli, A.**, Mukherjee, B., Hayakawa, R., Iwasaki, T., Nakaharai, S., & Wakayama, Y. (2020). Light-Assisted and Gate-Tunable Oxygen Gas Sensor Based on Rhenium Disulfide Field-Effect Transistors. Physica Status Solidi – Rapid Research Letters, 14(11), 2000330. https://doi.org/10.1002/pssr.202000330.

- Mukherjee, B., **Zulkefli, A.**, Watanabe, K., Taniguchi, T., Wakayama, Y., & Nakaharai, S. (2020). Laser‐Assisted Multilevel Non‐Volatile Memory Device Based on 2D van‐der‐Waals Few‐Layer‐ReS_2/h‐BN/Graphene Heterostructures. Advanced Functional Materials, 30(42), 2001688. https://doi.org/10.1002/adfm.202001688.

- Mukherjee, B., **Zulkefli, A.**, Hayakawa, R., Wakayama, Y., & Nakaharai, S. (2019). Enhanced Quantum Efficiency in Vertical Mixed-Thickness n-ReS_2/p-Si Heterojunction Photodiodes. ACS Photonics, 6(9), 2277-2286. https://doi.org/10.1021/acsphotonics.9b00580.